

The expected potential of hadronic PeVatron searches with spectral γ -ray data from the Southern Wide-field Gamma-ray Observatory

Ekrem Oğuzhan Angüner^a, Tülün Ergin^{b,c}

^aTÜBİTAK Research Institute for Fundamental Sciences, 41470 Gebze, Turkey

^bDepartment of Physics and Astronomy Michigan State University East Lansing MI USA

^cMiddle East Technical University Northern Cyprus Campus 99738 Kalkanlı via Mersin 10 Turkey

Abstract

The presence of a spectral softening, occurring at ~ 3 PeV energies, seen in the local cosmic-ray energy spectrum provides an evidence that our Galaxy hosts astrophysical objects, known as 'hadronic PeVatrons', that are capable of accelerating hadrons to PeV energies and above. Recent results from ground-based particle detector array experiments have provided conclusive evidence that these facilities are essential to explore the ultra-high-energy (UHE, $E > 100$ TeV) γ -ray domain and pinpoint the location of PeVatrons in the Galaxy. The Southern Wide-field Gamma-ray Observatory (SWGGO) is proposed next-generation ground-based extensive air shower observatory planned for construction in the Southern Hemisphere, which holds great scientific potential for UHE observations. In this study, we investigate the expected potential of SWGGO to search for hadronic PeVatrons, based on the publicly available preliminary SWGGO straw-man instrument response functions (IRFs). By using these straw-man IRFs, it can be shown that the SWGGO detection of γ -ray spectral cutoffs between 30 TeV and 100 TeV, at a 95% confidence level, is possible for faint γ -ray sources of ~ 5 mCrab given that the spectral index is hard ($\Gamma \lesssim 2.0$), while spectral cutoffs from softer sources with $\Gamma \cong 2.3$ can be detected for sources brighter than ~ 11 – 12 mCrab. The reconstructed SWGGO PeVatron detection maps demonstrate that the future SWGGO experiment can probe large parts of the investigated PeVatron parameter space, providing a robust detection and/or rejection of presence of spectral signatures associated with hadronic PeVatrons. A dedicated study on the promising Southern-sky PeVatron candidates, the Galactic Center region, Westerlund 1, HESS J1702–420 and HESS J1641–463, shows that the SWGGO will have a great potential to confirm or exclude PeVatron nature of these candidate sources at a robust significance level after 5-years of observation. In addition, it is shown that controlling systematic errors will be necessary to reach full potential of the SWGGO experiment for PeVatron searches.

Keywords: Gamma rays: general, Cosmic rays, Galactic PeVatrons, Methods: data analysis, Methods: statistical

1. Introduction

Cosmic Rays (CRs) are charged particles, roaming in our Galaxy with relativistic speeds and arriving the Earth's atmosphere isotropically from outer space. Decades of measurements have shown that the composition of CRs consist mainly of protons ($\sim 90\%$) followed by Helium nuclei ($\sim 9\%$), while the rest are heavier ions and electrons (see Blasi (2013); Amato (2014); Amato and Blasi (2018) for detailed review). The energy spectrum of CRs measured on Earth ranges from a few MeVs to beyond 10^{20} eV. Above ~ 30 GeV energies, it was historically described by a smooth power-law spectrum with an index of -2.7 up to the so called "knee" feature, emerging at ~ 3 PeV ($1 \text{ PeV} = 10^{15} \text{ eV}$), where the spectrum steepens significantly to -3.1 above these energies. When only the cosmic Hydrogen and Helium spectra are considered, there is an evidence that the respective knee is below 1 PeV, at energies around 700 TeV (ARGO-YBJ Collaboration et al., 2015). The detailed CR measurements have provided evidence of spectral

hardening around 100–300 GeV energies and re-softening at higher energies around ~ 100 TeV for all type of nuclei (Adriani et al., 2011; Aguilar et al., 2015b,a; Adriani and CALET Collaboration, 2022; Cardillo and Giuliani, 2023), especially for protons and Helium. These unique spectral characteristics suggest that a rigidity-dependent acceleration mechanism is at work in Galactic CR sources, allowing heavier nuclei to be accelerated to higher energies (Amato and Blasi, 2018; Amato and Casanova, 2021). Consequently, the knee feature observed in the CR spectrum can be interpreted as a sum of different nuclei types, each showing their unique cutoff in their respective spectra. As a result, the overall CR spectrum exhibiting more or less a smooth power-law up to 3 PeV energies provides a strong evidence that the sources in our Galaxy must accelerate CRs at least up to PeV energies and even well beyond. The existence of a "second knee" feature seen at ~ 100 PeV energies, which is thought to be originated from the heaviest nuclei, such as Fe ($Z=26$), further supports this idea (Schroder, 2019; Coleman, 2019; Cristofari, 2021). Given this scenario, it is believed that the second knee structure marks the lower bound of the energy region where transition from Galactic to the extra-galactic CRs occurs. Additionally, the recent detection of ultra-high-energy

Email address: oguzhan.anguner@tubitak.gov.tr (Ekrem Oğuzhan Angüner)

(UHE, $E > 100$ TeV) diffuse γ -ray emission from the Galactic plane (Amenomori et al., 2021a; Cao et al., 2023a) offers an alternative indirect way to study the distribution and propagation of global CRs in the Galaxy, when compared to local CR observations performed on Earth. More detailed reviews on the topic of CRs can be found in Amato (2014); Amato and Blasi (2018); Amato and Casanova (2021); Cristofari (2021); Di Sciascio (2022); Vink (2022); Casanova (2022).

In this context, the term "PeVatron" stands for astrophysical sources which can energize CRs at least up to PeV energies and beyond. Various astrophysical source classes, such as supernova (SN) Remnants (SNRs) (Bell, 1978; Gabici and Aharonian, 2007; Celli et al., 2019), massive star clusters (MSCs) (Aharonian et al., 2019; Morlino et al., 2021), core-collapse SNe (Tatischeff, 2009; Bell et al., 2013; Zirakashvili and Ptuskin, 2016; Marcowith and et al., 2018), pulsar wind nebulae (PWNe) (Amato, E. et al., 2003; Ohira et al., 2018; Guépin, Claire et al., 2020; Amato and Olmi, 2021), TeV halos (Linden et al., 2017; Fang, 2022), star formation regions (SFRs) (Bykov et al., 2020), microquasars (Abeysekara et al., 2018) and superbubbles (Higdon and Lingenfelter, 2003; Binns et al., 2005; Vieu et al., 2022), are expected to be promising PeVatron candidates. PeVatrons are categorized as "hadronic PeVatrons" or "leptonic PeVatrons" depending on whether the accelerated particles are primarily hadrons or leptons, respectively. The definition of PeVatron focuses on the maximum achievable energy of an accelerator, identifying the PeVatron nature based on the highest energy reached by individual particles at the acceleration site. This definition establishes a strict energy threshold of '1 PeV', distinguishing between PeVatron and non-PeVatron nature of the source, consequently making the 1 PeV energy threshold the primary property of a PeVatron. The detection of UHE γ -rays above 1 PeV from the Crab Nebula (LHAASO Collaboration et al., 2021), a known host of leptons with PeV energies for over a decade (Amato and Olmi, 2021), and the Cygnus Cocoon region (Cao and others, 2021), a superbubble surrounding a massive star formation region (Ackermann et al., 2011), implies the existence of particles accelerated to PeV energies at these sites, regardless of whether the emission has hadronic or leptonic origin, making the Crab Nebula and Cygnus Cocoon robust Galactic PeVatron sources according to the definition given above. The question of the origin of CRs, specifically the astrophysical accelerators capable of energizing CRs up to the observed knee feature around ~ 3 PeV energies, stands as one of the top scientific questions in astrophysics. Within this context, the investigation into the origin of CRs is directly linked to hadronic PeVatrons, as the contribution of leptons to the observed CR spectrum is negligible (~ 1 -2%). To account for the knee feature around ~ 3 PeV, CR sources must efficiently accelerate bulk of hadrons well beyond 1 PeV energies. Consequently, the hadronic spectrum produced by the accelerator should extend beyond 1 PeV energies without exhibiting a spectral cutoff.

From the experimental point of view, observed high-energy (HE, $E > 100$ MeV) and UHE γ -ray emission are the primary means to explore the origins of CRs. When γ -rays are created from proton-proton (pp) interactions followed by subsequent pion decay, the energy of γ -rays is typically around 10 times

lower than the energy of parent protons (Kelner et al., 2006; Kafexhiu et al., 2014; Celli et al., 2020), and can create spectral features in the γ -ray spectrum, providing clear signatures of hadronic interactions. For example, the AGILE and Fermi-LAT results (Giuliani, 2011; Ackermann, 2013) demonstrated that Galactic SNRs can accelerate CRs, producing low energy (MeV–GeV) γ -rays showing up as a "pion-bump" feature¹ in the observed SNRs' energy spectra. On the other hand, regardless of whether they are hadronic or leptonic, significant UHE emission is one of the main characteristics of PeVatron sources and must be detected for a robust claim of PeVatron nature. In the hadronic case, correlation with target material, in which accelerated particles can interact with, is expected. It is important to note that the target region, where CR interactions take place, is an evidence of PeVatron activity, but the region does not necessarily host the PeVatron source itself. In addition, neutrino emission is a clear indication of hadronic interactions (Kelner et al., 2006; Anchordoqui et al., 2014). However, the sensitivities of current neutrino experiments, i.e. IceCube (Abbasi and et al., 2009) and Baikal-GVD (Zabarov and the Baikal-GVD Collaboration, 2021), are not sufficient to put strong constraints on significant discrimination between hadronic and leptonic nature of PeVatrons (Abbasi et al., 2023), while the future neutrino observatories, such as IceCube-Gen2² and KM3NeT³, are expected to reach such high sensitivities.

The first indication of the presence of a Galactic PeVatron at the Galactic center (GC) region is discussed in HESS Collaboration et al. (2016). Detection of the GC PeVatron was claimed based on the derived 95% confidence level (CL) lower limits on the parent proton spectral cutoff of 0.4 PeV, together with the strong correlation observed between the very-high energy (VHE, $0.1 \text{ TeV} < E < 100 \text{ TeV}$) γ -ray emission and distribution of molecular gas. After this pioneering study, interpreting PeVatron nature of a source based on 95% CL lower limits of the proton spectral cutoff became a standard approach in PeVatron searches (Spengler, G., 2020; Abdalla, H. et al., 2021). In the following years, ground-based water Cherenkov detector (WCD) experiments, Tibet AS-gamma (Amenomori et al., 2019, 2021b) and the High-Altitude Water Cherenkov Observatory (HAWC) (Abeysekara et al., 2020), reported significant detection of Galactic UHE photons and sources, respectively. Finally, the discovery of 12 Galactic UHE source by the LHAASO collaboration marked a major milestone in PeVatron searches, and completely reshaped our understanding of the PeVatron concept, as many of these sources are plausibly associated to leptonic accelerators like pulsars and PWNe (Cao and others, 2021). The recently published first LHAASO catalogue of γ -ray sources have revealed 43 UHE sources detected above 100 TeV with significance greater than 4σ (Cao et al., 2023b).

These experimental results have provided clear evidence that ground-based WCDs, e.g. HAWC and LHAASO, due to their

¹The pion bump is a characteristic spectral feature observed in the spectral energy distribution of γ rays, seen in between 100 MeV and 1 GeV energies. This feature is a result of hadronic interactions between accelerated CRs with the surrounding gas. Please refer to Yang, R. et al. (2018) for more details.

²https://www.icecube-gen2.de/index_eng.html

³<https://www.km3net.org/>

enhanced high energy flux sensitivities above ~ 10 TeV, are the key facilities to explore the UHE regime and locate PeVatrons in the Galaxy, therefore making them "PeVatron hunters". However, up to date, no Galactic source that has been firmly proven to accelerate hadrons to PeV energies and above could be identified. This is due to the fact that discrimination between hadronic and leptonic PeVatrons, using current observational data, are extremely challenging. On the other hand, angular resolution of WCD experiments ($\sim 0.2^\circ$ - 0.3°) is a factor of 3–4 worst when compared to current generation imaging atmospheric Cherenkov telescopes (IACTs). Such a disadvantage causes source confusion to become a major problem for the ground-based WCD observations, consequently making it impossible to pin down the astrophysical origin of the observed emission from morphology studies. The synergy between future VHE and UHE γ -ray instruments such as the Cherenkov Telescope Array (CTA) (Acharya and et al., 2013; Hofmann and Zanin, 2023) and the Southern Wide-field Gamma-ray Observatory (SWGGO) (Albert, A. et al., 2019) will play a critical role for robust identification of Galactic PeVatrons which can contribute significantly to the CR knee feature. In addition, future neutrino experiments, like KM3NeT and IceCube-Gen2, will be able to provide sensitive measurements that can resolve the ambiguity between leptonic and hadronic PeVatrons. More detailed reviews on the topic of PeVatrons can be found in Amato and Casanova (2021); Amato and Blasi (2018); Amato (2014); Di Sciascio (2022); Casanova (2022); Cristofari (2021); Vink (2022); Sudoh and Beacom (2023); la Fuente et al. (2023); Cardillo and Giuliani (2023); Angüner (2023); Cao et al. (2023c).

Throughout this paper, we focus on the hadronic PeVatrons, namely source of CRs at energies around the knee of the CR spectrum. Consequently, the leptonic PeVatrons are out of the scope of this study. The paper is structured as follows. The next-generation SWGGO experiment is briefly introduced in Sec. 2. Simulations of the SWGGO observations and the data analysis methods employed in this study are discussed in Sec. 3. The results on the investigation of SWGGO's sensitivity in γ -ray spectral cutoff detection are provided and discussed in Sec. 4. The general ability of SWGGO to identify PeVatron sources is quantified in Sec. 5. Simulation results of the SWGGO observations of the promising PeVatron candidates in the Southern-sky are provided and discussed in Sec. 6. Finally, the discussions and conclusions are summarized in Sec. 7.

2. The Southern Wide-field Gamma-ray Observatory

SWGGO is a proposed next-generation ground-based Extensive Air Shower (EAS) observatory to be built in the Southern Hemisphere, designed to scan large parts of the sky with a large field of view (FoV) at a very high duty cycle ($>95\%$), and measure γ -rays within the range spanning from a few hundred GeVs to PeV energies (Albert, A. et al., 2019). Expected to start full operations by 2026, SWGGO is set to maintain its operational capacity for a minimum of 10 years. The fundamental structure of SWGGO consists of ground-based WCDs, positioned in the Southern Hemisphere at an altitude exceeding 4400 m above sea level (Conceição and SWGGO Collaboration, 2023; Barres

de Almeida and SWGGO Collaboration, 2022). These WCDs are designed to optimize and enhance both signal collection and particle recognition capabilities through the exceptionally precise time resolution ($\Delta t \approx 2$ ns) and advanced signal reconstruction techniques, respectively. One of the proposed detector designs is a dual-layered water Cherenkov tank, which will enable reconstructing the number of muons and separating primary CRs, therefore both increasing the background rejection rate and allow CR anisotropy measurements (Lang and SWGGO Collaboration, 2023), respectively.

The scientific potential and capabilities of ground-based EAS arrays have already been demonstrated by the current generation observatories like HAWC (Abeysekera, A.U. et al., 2017) and LHAASO (Vernetto and for the LHAASO Collaboration, 2016), both of which are located in the Northern Hemisphere. Despite the Southern-sky holds great scientific potential, there is currently no operational EAS observatory in the Southern Hemisphere. In this regard, SWGGO will serve as a complementary to the currently existing ground-based EAS observatories in the Northern Hemisphere, and to the next-generation IACT project, the CTA observatory. Through a five-year data collection with SWGGO, it is expected that the sensitivity of detecting point-like γ -ray sources at energies exceeding 10 TeV will be better when compared to 50 hours of CTA data (Albert, A. et al., 2019). This advantage, together with its large FoV, makes SWGGO an ideal observatory to search for γ -ray sources above several 10 TeV. Such capability is particularly important for revealing sources of Galactic CR acceleration and the systematic investigation of transient events at these high energies. Furthermore, SWGGO has the potential to play a key role in subsequent follow-up observation campaigns in case of transient alerts and multi-messenger triggers, both by mapping the distribution of transient and by extending the simultaneous sky coverage of γ -ray monitoring facilities, e.g. HAWC, LHAASO, and CTA (La Mura et al., 2020), respectively. In addition, strategic location of SWGGO close to the Southern Tropic (Albert, A. et al., 2019) ensures efficient coverage of the declination band of transient events that might be associated to neutrino alerts from current neutrino observatories, e.g. IceCube⁴ (Meneguolo et al., 2023), future neutrino observatories like KM3NeT and IceCube-Gen2, and gravitational wave observatories, such as LIGO⁵ (Magee and et al., 2021).

The search for the location of the SWGGO construction site has been in progress as a part of the research and development phase, and is expected to reach its conclusion by the end of 2024. Up to date, the SWGGO collaboration has been systematically gathering detailed information regarding the potential sites under consideration, which are located in Argentina, Chile, and Peru (Doro and SWGGO Collaboration, 2022). The selection of these candidate sites was based on various factors including altitude, local topology, environmental conditions, site access, transport costs, as well as the availability and cost of essential resources like water, power, and network connectivity (Santander and SWGGO Collaboration, 2023).

⁴<https://icecube.wisc.edu/science/real-time-alerts/>

⁵https://emfollow.docs.ligo.org/userguide/early_warning.html

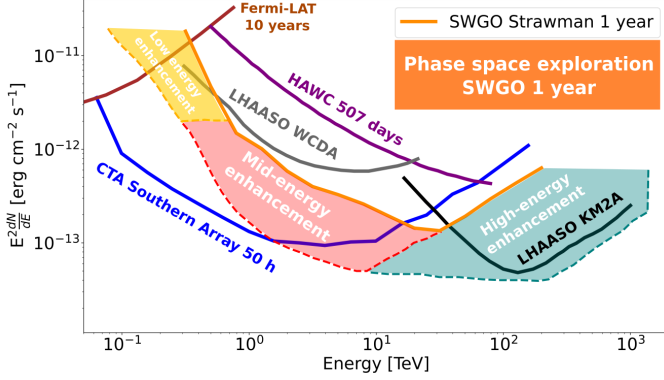


Figure 1: A comparison of differential point-like source sensitivities between the SWGO (the 1 year straw-man, solid-orange, taken from Albert, A. et al. (2019)), Fermi-LAT (10 years P8R3_SOURCE_V3, solid-brown, taken from Ajello et al. (2021)), CTA (50 h Southern array prod5.v0.1, solid-blue, taken from CTA Observatory and Consortium (2021)), HAWC (507 days, solid-magenta, taken from Abeyssekara, A.U. et al. (2017)) and LHAASO WCDA (1 year, solid-gray) and LHAASO KM2A (1 year, solid-black) taken from Chen et al. (2022); della Volpe (2023). The yellow, red and blue shaded bands indicate the foreseen phase-space exploration of the low-energy, mid-energy and high-energy enhancement, respectively, for the SWGO experiment. The figure is adapted from Hinton and SWGO Collaboration (2022).

Figure 1 shows the differential point-like source sensitivity curves from various experiments, along with the sensitivity of the SWGO for 14 different detector and array layout configurations, which are indicated with shaded bands featuring different colors. The selection of these configurations follows a detailed investigation of array and detector parameters, including dimensions of the detector station, number and size of photo-sensors placed inside the detector, and the distribution of the dense inner (for lower energies) and sparse outer array (for higher energies), as well as the correspondence between them. The solid orange sensitivity curve shown in Fig. 1 represents the preliminary baseline configuration of SWGO, which is referred as the **straw-man design** throughout this paper. This straw-man design configuration comprises a compact inner array with a 160 m radius and a fill factor of $\sim 80\%$, which is surrounded by a less dense outer array, having a radius of 300 m and a fill factor of $\sim 5\%$. The detector units in both the inner and outer arrays, resembling a two-compartment cylindrical tank with a diameter of 3.8 m, are identical and resulting in a total of 6600 detector units (Schoorlemmer and SWGO Collaboration, 2022). The sensitivity of the straw man design was evaluated between 20 GeV up to 500 TeV by extrapolating the published HAWC performance metrics (Abeyssekara, A.U. et al., 2017), such as the angular and energy resolution to be $\sim 0.15^\circ$ and $\sim 25\%$ at 30 TeV, respectively, as well as the passing rate of the gamma and hadron cut to be $\sim 2 \times 10^{-3}$ (see Fig. 11 of Abeyssekara, A.U. et al. (2017)).

The sensitivity curve of SWGO shown in Fig. 1 serves as a guiding reference to direct the design studies, rather than being a definite measure of SWGO performance. The comprehensive exploration of the complete parameter phase-space is expected to be completed in 2024. The differently colored shaded regions in Fig. 1 represent various design options aimed at improving

the sensitivity of the straw man design. Potential enhancements in low-energy performance (shaded yellow region) are achievable by lowering the individual unit thresholds and the exploration of higher elevation sites. In the mid-energy range (shaded red region), it has been shown that significant enhancements in both angular resolution and background rejection can be achieved (Hofmann, 2020; Kunwar, 2021; Conceição et al., 2021). The lower limit of the color band, marked by the dashed line, corresponds to a 30% improvement in the point spread function (PSF) and a tenfold increase in background rejection efficiency. Particularly, ongoing investigations focus on compact detector units with dedicated muon tagging capabilities to further enhance background rejection efficiency. For the high-energy range (shaded blue region), performance improvements can be achieved by implementing a low-density, large outer array with a size of a few square kilometers, coupled with effective background rejection capabilities. As it was evident from the LHAASO results (Cao and others, 2021), it is possible to implement a square kilometer array with a background efficiency of $\sim 10^{-5}$. These studies will provide valuable insights for identifying the most favorable SWGO design configurations to consider, subsequently followed by the production of the official SWGO instrument response functions (IRFs). Therefore, we explicitly mention that the results and conclusions presented throughout this paper are not based on any official IRFs or tools provided by the SWGO collaboration. Additionally, the results and conclusions derived in this paper are conservative with regard to their dependence on the assumed differential sensitivity.

3. Simulations and data analysis

The expected potential of identifying point-like PeVatron sources using the forthcoming SWGO experiment data is evaluated through Monte-Carlo (MC) simulations, based on the differential straw-man sensitivity⁶ outlined in Albert, A. et al. (2019). This straw-man SWGO sensitivity curve is provided with an energy binning approach. Each bin, indexed with i and centered at the energy value of E_i , in principle, determines the minimum detectable γ -ray flux level $\Phi_{\text{Sens}}(E_i)$ within it, ensuring a 5σ detection significance, assuming observation times of both 1 year and 5 years. For each specific E_i , the simulated γ -ray flux points $\Phi(E_i)$ are generated based on SWGO straw-man sensitivity curve with $\sigma(E_i) = \Phi_{\text{Sens}}(E_i)/5$ as the standard deviation, and are distributed normally around $\Phi_{\text{True}}(E_i)$ representing the predicted γ -ray spectrum from astrophysical sources. Spectral data points exhibiting a relative error $\sigma(E_i)/\Phi(E_i)$ exceeding 100% are excluded from subsequent analyses. This exclusion is due to the intention of deriving flux upper limits for such data points in practical analysis applications.

In the subsequent sections, either the simulated SWGO γ -ray flux data or publicly available spectral γ -ray flux data obtained from H.E.S.S. observations of various Galactic PeVatron candidate sources are analyzed within the framework of `gammapy`

⁶The differential straw-man sensitivity curve data are taken from <https://github.com/harmscho/SGSOSensitivity>.

(Deil et al., 2020). The analysis procedure is based on fitting the respective flux data sets to γ -ray emission models. The model parameters that best describe the data are determined by minimizing the χ^2 statistic.

When dealing with the publicly available H.E.S.S. flux data, which may include asymmetric statistical errors represented by $[\sigma_-, \sigma_+]$, the symmetric statistical errors given by $\sigma_{\text{stat}} = \max\{\sigma_-, \sigma_+\}$ are conservatively adapted instead of directly incorporating the asymmetric errors. Additionally, relative systematic flux error of $\sigma_{\text{sys}} = \xi dN/dE$ with $\xi=20\%$ is taken into account for the H.E.S.S. data (Aharonian et al., 2006). To explore the potential impact of systematic errors on the PeVatron searches with SWGO, relative systematics of $\xi=5\%$ (optimistic case) and $\xi=10\%$ (conservative case) are assumed in the simulated SWGO flux points. These assumptions are based on the 7% flux systematics observed in the LHAASO experiment (Aharonian et al., 2021). Finally, the overall error associated with the analyzed flux data points is determined by selecting the larger value as $\sigma = \max\{\sigma_{\text{sys}}, \sigma_{\text{stat}}\}$. This combined error estimation ensures a conservative consideration of the uncertainties in the analysis.

The differential spectrum of γ -ray sources are modeled as exponential cutoff power law (ECPL) model formulated as follows

$$\Phi_{\text{ECPL}}(E) = \Phi_0(E_0) \cdot \left(\frac{E}{E_0}\right)^{-\Gamma_\gamma} \cdot \exp(-\lambda_\gamma E), \quad (1)$$

where $\lambda_\gamma=(1/E_{\text{cut},\gamma})$ is the inverse γ -ray cutoff energy with $E_{\text{cut},\gamma}$ representing the cutoff energy of γ -ray spectrum, Γ_γ is the spectral index and $\Phi_0(E_0)$ is the source flux normalization at the reference energy E_0 . Likewise, the differential energy distribution of accelerated protons is also assumed to follow an ECPL model expressed as

$$J_p(E_p) \sim E_p^{-\Gamma_p} \exp\left(-(\lambda_p E_p)^\beta\right), \quad (2)$$

where $\lambda_p=(1/E_{\text{cut},p})$ is the inverse proton cutoff energy $E_{\text{cut},p}$ and Γ_p is the proton spectral index. The parameter β describes the degree of sharpness in the exponential cutoff, and for the analyses presented in this paper, it is fixed to $\beta=1$. This choice adequately captures the particle spectra characteristics in scenarios involving hadronic acceleration as discussed in Schure and Bell (2013); Cristofari et al. (2020); Angüiner et al. (2023). The likelihood test statistics,

$$\text{TS}_{\gamma,p} = -2 \ln \frac{\hat{L}(\lambda_{\gamma,p} = 0)}{\hat{L}(\lambda_{\gamma,p})}, \quad (3)$$

where $\hat{L}(\lambda_{\gamma,p})$ and $\hat{L}(\lambda_{\gamma,p} = 0)$ are the maximum likelihoods over the full parameter space, either for γ -rays ($\lambda_\gamma, \Phi_0, \Gamma_\gamma$) or protons ($\lambda_p, \Phi_0, \Gamma_p$), used for quantifying the statistical significance of γ -ray spectral energy cutoffs ($S_{\text{cut},\gamma} = \sqrt{\text{TS}_\gamma}$) and protons spectral cutoffs ($S_{\text{cut},p} = \sqrt{\text{TS}_p}$), respectively. The PeVatron Test Statistics (PTS) method, as introduced in Acero, F. et al. (2023) and formulated as

$$\text{PTS} = -2 \ln \frac{\hat{L}(E_{\text{cut},p} = 1 \text{ PeV}, \theta|D)}{\hat{L}(E_{\text{cut},p}, \theta|D)}, \quad (4)$$

offers a likelihood ratio test that enables the measurement of the deviation of the best-fit hadronic energy cutoff, denoted as $E_{\text{cut},p}$, extracted from a specific set of observed data (D), from a fixed proton cutoff energy threshold set at 1 PeV. Throughout this paper, only flux data $\Phi(E_i)$ with errors $\sigma(E_i)$ in energy bins E_i are analyzed, and the adopted likelihood function is given by

$$L(E_{\text{cut},p}, \theta|D) = -2 \sum_i \left(\frac{\Phi_\gamma(E_i|E_{\text{cut},p}, \theta) - \Phi(E_i)}{\sigma(E_i)} \right)^2, \quad (5)$$

where $\theta = (\Gamma_p, \Phi_{0,p})$. This paper consistently employs the statistical significance of the PTS ($S_{\text{PTS}} = \text{sign}(E_{\text{cut},p} - 1 \text{ PeV}) \sqrt{\text{PTS}}$) to gauge the level of statistical significance regarding the identification of spectral PeVatron signatures. The `ecpli` package (Spengler, G., 2022) is used to derive lower limits for both hadronic and γ -ray cutoff energies associated to a given source, following the methods as explained comprehensively in the appendix provided in Acero, F. et al. (2023). The analysis presented in this paper does not include the impact of the attenuation of γ -ray emission due to pair creation, i.e. the process $\gamma\gamma \rightarrow e^+e^-$. This exclusion is due to the focus on simulated spectral γ -ray flux points with energies below 200–300 TeV. As outlined in Vernetto and Lipari (2016), it is assumed that the flux attenuation due to pair creation is negligible ($< 10\%$) below these energies. Nevertheless, it is important to mention that when simulating SWGO data without accounting for systematic errors ($\xi = 0$), the impact of pair creation can become significant, particularly depending on the location of the source in the Galaxy and its distance.

4. Investigating SWGO's sensitivity in γ -ray spectral cutoff detection

The SWGO Collaboration has defined a set of science benchmarks, encompassing the key target scientific objectives of the SWGO project, with the aim of exploring performance parameters that are crucial for the best possible optimization of the forthcoming SWGO experiment (Hinton and SWGO Collaboration, 2022). One of them is directly related to PeVatron searches and defined under the 'Galactic accelerators' science case. The benchmark is described as "Maximum exponential-cutoff energy detectable at 95% CL in 5 years for a γ -ray source with spectral parameters of $\Phi_0(1 \text{ TeV})=5 \text{ mCrab}^7$ and $\Gamma_\gamma=2.3$ " (Hinton and SWGO Collaboration, 2022). In this section, results of a dedicated simulation study utilizing 5-years straw-man SWGO sensitivity curve are presented. The aim of this study is to explore and provide an estimation of the maximum detectable energy cutoff at a 95% CL over a 5-year observation time as defined in the respective SWGO science benchmark.

In principle, detecting a γ -ray spectral cutoff, or equivalently, robust determination of a spectral shape, requires reasonably broad energy coverage and sufficient event statistics within that

⁷The Crab unit is taken as the differential Crab flux level at 1 TeV of $3.84 \times 10^{-11} \text{ cm}^{-2} \text{ s}^{-1} \text{ TeV}^{-1}$ following Table 6 of Aharonian et al. (2006)

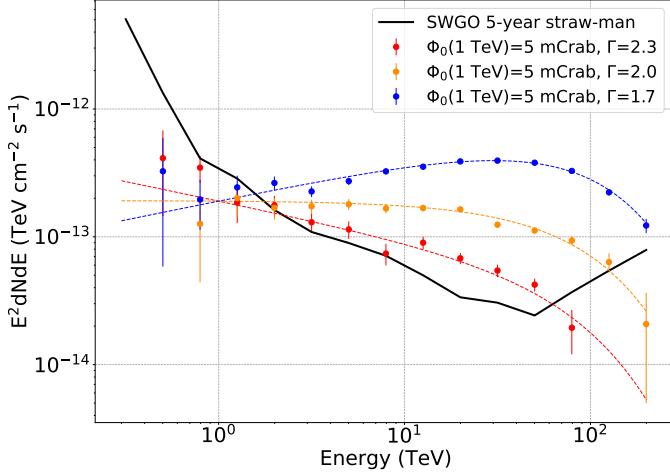


Figure 2: A comparison is shown between γ -ray spectral models with different spectral indices of $\Gamma=2.3$ (red), $\Gamma=2.0$ (yellow) and $\Gamma=1.7$ (blue), for a source exhibiting a flux normalization Φ_0 of 5 mCrab at 1 TeV, and a fixed γ -ray spectral cutoff energy of 100 TeV. Additionally, the flux points derived from SWGO simulations, following the procedure detailed in Sec. 3, are shown in their corresponding colors, accounting only for 1σ statistical errors ($\xi = 0$). The solid black line outlines the 5-year SWGO straw-man sensitivity curve.

energy range. Figure 2 illustrates a comparison between different γ -ray spectral models with various spectral indices, originating from a 5 mCrab source exhibiting a 100 TeV γ -ray spectral cutoff, together with the simulated respective SWGO flux points following the method detailed in Sec. 3. The figure clearly reveals that detecting a 100 TeV γ -ray cutoff from a 5 mCrab and $\Gamma=2.3$ source (dashed red line) encounters challenges due to both insufficient statistics and the limited ability of the SWGO 5-year straw-man sensitivity curve to effectively capture the cutoff feature. Conversely, a source with a comparable flux level but showing a harder spectral index of $\Gamma=1.7$ benefits from comprehensive coverage, making the detection of a 100 TeV cutoff feature possible. A preliminary investigation of the simulated 5 mCrab and $\Gamma=2.3$ source did not conclusively result in a detection of any spectral cutoff feature up to energies of 300 TeV at a 95% CL. Consequently, the simulation study is extended further to production of spectral detection maps, introduced in Acero, F. et al. (2023), which encompass a wide range of the γ -ray spectral parameter space and can be used to investigate the detectable cutoff energies at a desired CL.

Figure 3 shows the reconstructed γ -ray spectral cutoff detection map using 5-years of SWGO observations for a fixed flux normalization of $\Phi_0(1 \text{ TeV})=5 \text{ mCrab}$ (left) and a fixed γ -ray spectral index of $\Gamma=2.3$, together with 95% CL contour lines assuming $S_{\text{cut},\gamma}=5\sigma$ (yellow) and $S_{\text{cut},\gamma}=3\sigma$ (black) cutoff detection thresholds given in Eq. 3, respectively. As evident from the figures, the reference source cited in the SWGO science benchmark fails to achieve a 95% CL detection for any spectral cutoff value spanning from 10 to 300 TeV when taking the straw-man design sensitivity curve into account. By analyzing the characteristics of the reference source parameters separately, it becomes apparent that γ -ray spectral cutoff energies ranging from 30 to 100 TeV can be confidently detected (at 5σ level)

for a 5 mCrab source, given that the γ -ray spectral index is hard ($\Gamma \leq 2.0$). The probabilities of detecting these cutoff energies exhibit a relatively flat structure between 30 TeV and 100 TeV. On the other hand, when considering γ -ray sources with a spectral index of $\Gamma=2.3$, robust detection of their spectral cutoffs can become possible only if the flux $\Phi_0(1 \text{ TeV})$ is larger than $\sim 11 \text{ mCrab}$. In this case, the capability to identify spectral cutoffs attains its peak performance at $E_{c,\gamma} \sim 30 \text{ TeV}$, and the maximum energy at which a cutoff can be detected increases as the source gets brighter. If a less strict cutoff detection threshold of $S_{\text{cut},\gamma}=3\sigma$ is assumed, the minimum prerequisites for spectral parameters become less conservative, enabling the potential detection of spectral cutoffs even for a 5 mCrab source with $\Gamma \sim 2.1$, as well as for a $\sim 8 \text{ mCrab}$ and $\Gamma=2.3$ source.

5. Exploration of PeVatron parameter space

As it was discussed in Acero, F. et al. (2023); Angüner (2023), it is important to highlight that establishing a direct relationship between the 'detection or absence of γ -ray spectral cutoffs' and the 'identification of PeVatron spectral signatures' is not always straightforward. Indeed, the presence of a significant γ -ray spectral cutoff observed at UHEs (i.e. $E > 100 \text{ TeV}$) could potentially be interpreted as a sign of PeVatron detection assuming that the observed γ -ray emission originates from hadronic interactions. Conversely, a source that does not exhibit a clear γ -ray spectral cutoff within the energy range of the instrument, i.e. due to its very high underlying hadronic spectral cutoff, would clearly display a more promising spectral PeVatron signature, only if this spectral behaviour is significant. The recently introduced PTS method (Acero, F. et al., 2023) offers a gauge to quantitatively assess the statistical significance of such spectral behaviors.

In this section, the potential of SWGO observations to decide whether a given source is associated with a PeVatron or not is estimated based on the straw-man design configuration for general point-like γ -ray sources, assuming 1 year and 5 years of simulated SWGO observations. The investigation encompasses a wide range of parameters, denoted as Φ_0 which corresponds to true γ -ray flux observed from Earth, resulting from pp interactions followed by subsequent π^0 decay, and proton spectral index Γ_p , associated with PeVatron sources. The SWGO flux points are simulated using γ -ray emission models from hypothetical PeVatrons characterized by a proton cutoff energy of $E_{\text{cut},p} = 3 \text{ PeV}$, as well as from non-PeVatron sources having a proton cutoff energy of $E_{\text{cut},p} = 300 \text{ TeV}$, taking into account various combinations of (Φ_0, Γ_p) parameters. Since SWGO's sensitivity is expected to be more pronounced at higher energies ($E \gg 1 \text{ TeV}$, see Fig. 2), the flux normalization of the maps is established at a reference energy of 10 TeV, deviating from the typical value of 1 TeV generally used in VHE astronomy. The probability to detect a PeVatron and, respectively, to exclude that a hadronic γ -ray source is a PeVatron, with a statistical significance of more than robust $S_{\text{PTS}}=5\sigma$ level, is estimated by taking the fraction of simulated sources for which the PTS is larger than 25 and, respectively, smaller than -25 as it was discussed and detailed in Acero, F. et al. (2023); Angüner (2023).

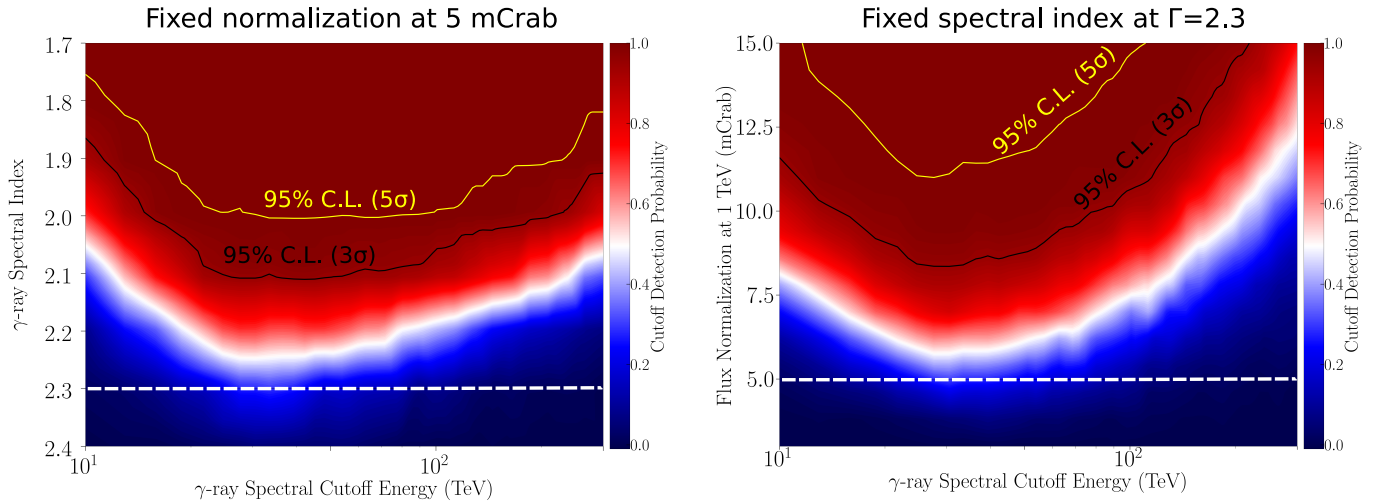


Figure 3: The γ -ray spectral cutoff detection maps reconstructed from 5-years of SWGO observations are shown for a fixed flux normalization of $\Phi_0(1 \text{ TeV})=5 \text{ mCrab}$ (left) and for a fixed gamma-ray spectral index of $\Gamma=2.3$ (right). The x-axes show γ -ray spectral cutoff energies, while the y-axes show the γ -ray spectral index (left) and flux normalization at 1 TeV (right) of the simulated ECPL model given in Eq. 1, respectively. For the reconstruction of the cutoff energy axis, a total of 29 equally spaced logarithmic bins between 10 and 300 TeV energies have been used. As for the spectral index and flux normalization axes, eight bins cover the range of $\Gamma=[1.7, 2.4]$, and 13 bins cover the flux range of $\Phi_0(1 \text{ TeV})=[3.0, 15.0] \text{ mCrab}$, respectively. Within each $(\Phi_0, \Gamma, E_{c,\gamma})$ combination bin, a set of 500 simulations of SWGO flux points is performed based on the corresponding γ -ray model, and the distribution of TS_γ is generated. The detection probabilities of the spectral cutoffs, represented on the z-axis, are calculated by assuming a cutoff detection threshold of $TS_\gamma \geq 25$ (5σ) and taking the fraction of the distribution above this threshold, as initially introduced in (Acero, F. et al., 2023). The yellow and black contours indicate lower bounds of the parameter space in which the 95% CL cutoff detection can be established assuming the cutoff detection threshold of $S_{\text{cut},\gamma}=5\sigma$ and $S_{\text{cut},\gamma}=3\sigma$, respectively. The white dashed lines in figures indicate location of the reference source cited in SWGO science benchmark, with parameters of $\Phi_0(1 \text{ TeV})=5 \text{ mCrab}$ and $\Gamma=2.3$, on the phase space.

Figure 4 shows the SWGO PeVatron detection (right panels) and exclusion (left panels) maps, revealing that the sensitivity achieved with the SWGO straw-man design configuration is already promising for exploring significant portions of the investigated parameter space of PeVatron sources. For the purpose of relative performance comparison with future VHE experiments, such as the CTA (Acero, F. et al., 2023), similar maps reconstructed using the flux normalization at Φ_0 at 1 TeV (in mCrab units) are also provided in Appendix A. Considering the straw-man design configuration, it becomes evident that the PeVatron detection capability of SWGO after 1 year of observations is comparable to what can be achieved with 50 hours of CTA observations. Consequently, 1-year SWGO observations can provide much higher PeVatron detection sensitivity with respect to what can be expected from the planned CTA scan of the Galactic plane (Cherenkov Telescope Array Consortium et al., 2019; Abe et al., 2023), which is estimated to have an average exposure of ~ 10 hours. Moreover, extending observations to 5 years with SWGO yields a relatively better PeVatron detection sensitivity compared to 100 hours of deeper follow-up CTA observations. However, this comparison neglects the fact that a source which appears as point-like for SWGO, considering its angular resolution of $\sim 0.15^\circ$ above 30 TeV, will indeed not display point-like characteristics for the CTA due to its superior angular resolution. It is important to point out that the comparison based on the analysis results do not include systematic errors. The conclusions can change depending on the extent of systematic uncertainties. The power of PeVatron detection and exclusion, derived from observations with SWGO as shown in

Fig. 4 (and also in Fig. A.7), diminishes by a factor of 2–8, depending on the source brightness and spectral index, when a conservative systematic flux error of $\xi = 10\%$ is assumed. The effect is more pronounced for the weak and soft sources, consequently shifting the transition regions⁸ to higher flux levels. This confirms that the control of systematic errors is an important prerequisite to reach the full potential of SWGO.

6. Probing promising PeVatron candidates of the Southern-sky with SWGO

In this section, the analysis results of SWGO simulations based on the public spectral γ -ray data from four promising Southern-sky Galactic PeVatron candidate sources, the GC diffuse emission⁹ region at the center of the Galaxy (HESS Collaboration et al., 2016), the young massive stellar cluster Westlund 1 (Aharonian, F. et al., 2022), and unidentified hard γ -ray sources HESS J1702–420A (Abdalla, H. et al., 2021) and HESS J1641–463 (Abramowski et al., 2014a), are presented and discussed in the framework of the SWGO straw-man configuration design. All four of these γ -ray sources detected at VHEs are considered as promising $E > 100 \text{ TeV}$ emitters, either

⁸Transition region is the part of the parameter space in which the detection (or exclusion) probabilities are between 0.5 and 0.9 contour lines.

⁹The GC diffuse emission spectrum is extracted from an annulus centred at Sgr A* (see right panel of Fig. 1 in HESS Collaboration et al. (2016)) with inner and outer radius of 0.15° and 0.45° , respectively, and a solid angle of $1.4 \times 10^{-4} \text{ sr}$.

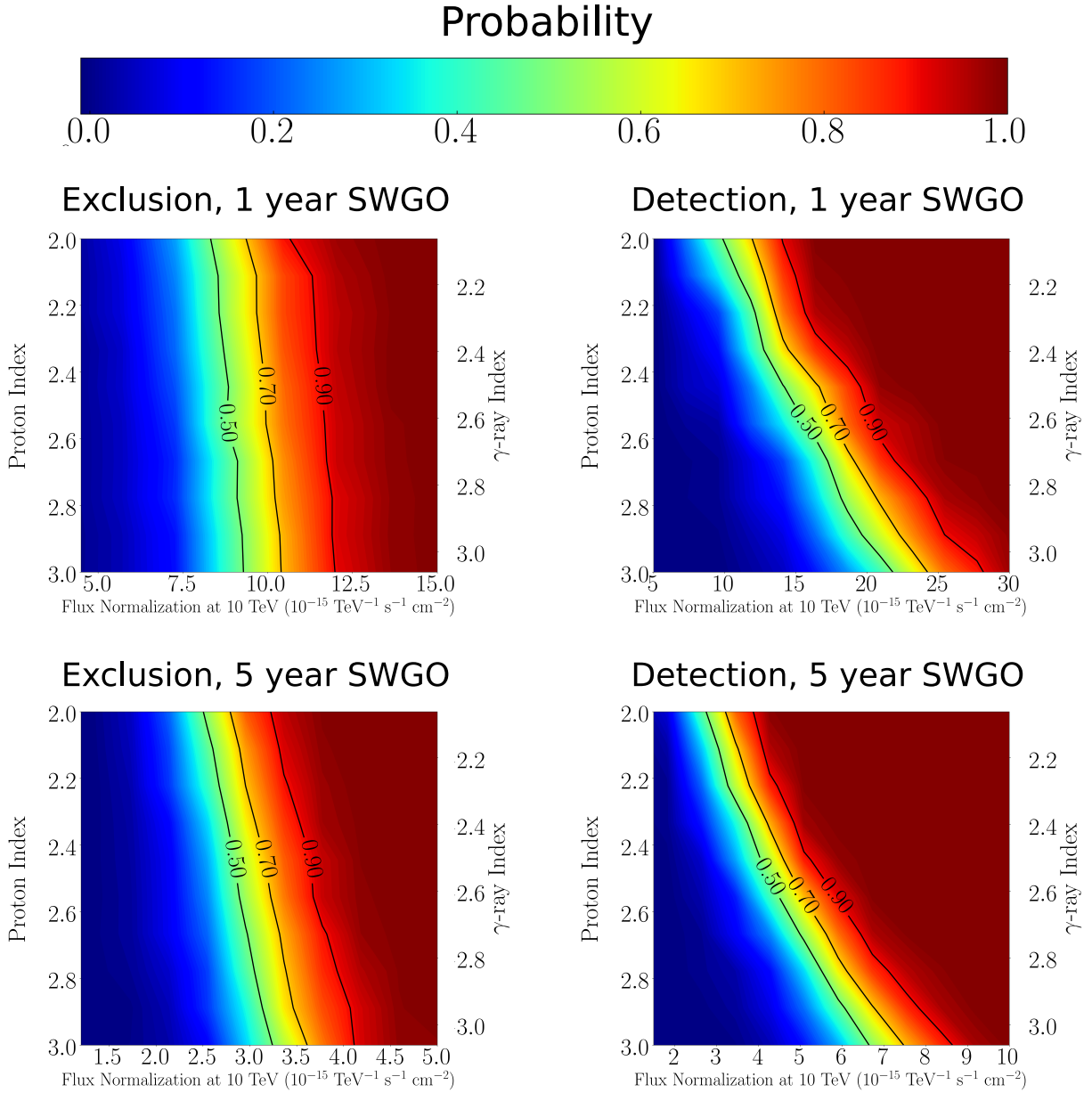


Figure 4: Estimated probability maps for exclusion (left panels) and detection (right panels) of a PeVatron source with a robust statistical significance of 5σ with SWGO data. This estimation is based on the assumed SWGO straw-man sensitivity curve (Albert, A. et al., 2019) taken from <https://github.com/harmscho/SGSOSensitivity>. The reconstruction of maps follows the methodology introduced in Acero, F. et al. (2023). The x-axis and the left and right y-axes represent the assumed parameter values for the true observed γ -ray flux normalization Φ_0 at 10 TeV originating from pp interactions observed from Earth, the spectral index of the hadronic particle distribution (Γ_p), and the corresponding spectral index of ECPL γ -ray emission (Γ_γ), respectively. The color bar indicates the probability of either exclusion (left panels) or detection (right panels) of a PeVatron with a statistical significance of 5σ , using the PTS method. The top panels present the results for 1 year of SWGO observations, whereas the bottom panels shows 5 year observations. The cutoff energy for the hadronic particle spectrum in the left panels, representing exclusion power at a 5σ significance for non-PeVatron sources, is assumed to be $E_{\text{cut},p}=300$ TeV. On the other hand, $E_{\text{cut},p}=3$ PeV is used for the right panels, which demonstrate SWGO’s power to robust detection of a PeVatron. The contours representing detection and rejection probabilities of 0.5, 0.7, and 0.9 are shown with solid black lines.

due to their fluxes detected at high-energies (such as ~ 81 TeV for Westerlund 1 and ~ 85 TeV for HESS J1702–420A) or from their observed power-law characteristic that exhibit hard spectral features without showing any clear indications of spectral cutoffs (GC diffuse emission region and HESS J1641–463). Such unique spectral features, which are listed in Table 1, make

these sources particularly intriguing as potential Southern-sky PeVatron candidates, as the possibility of hadronic emission scenarios cannot be ruled out for any of them. Location of these Southern-sky PeVatron candidates are marked with green dots in the SWGO Southern-sky visibility plot shown Fig. 5. As illustrated, all of these sources can be observed under

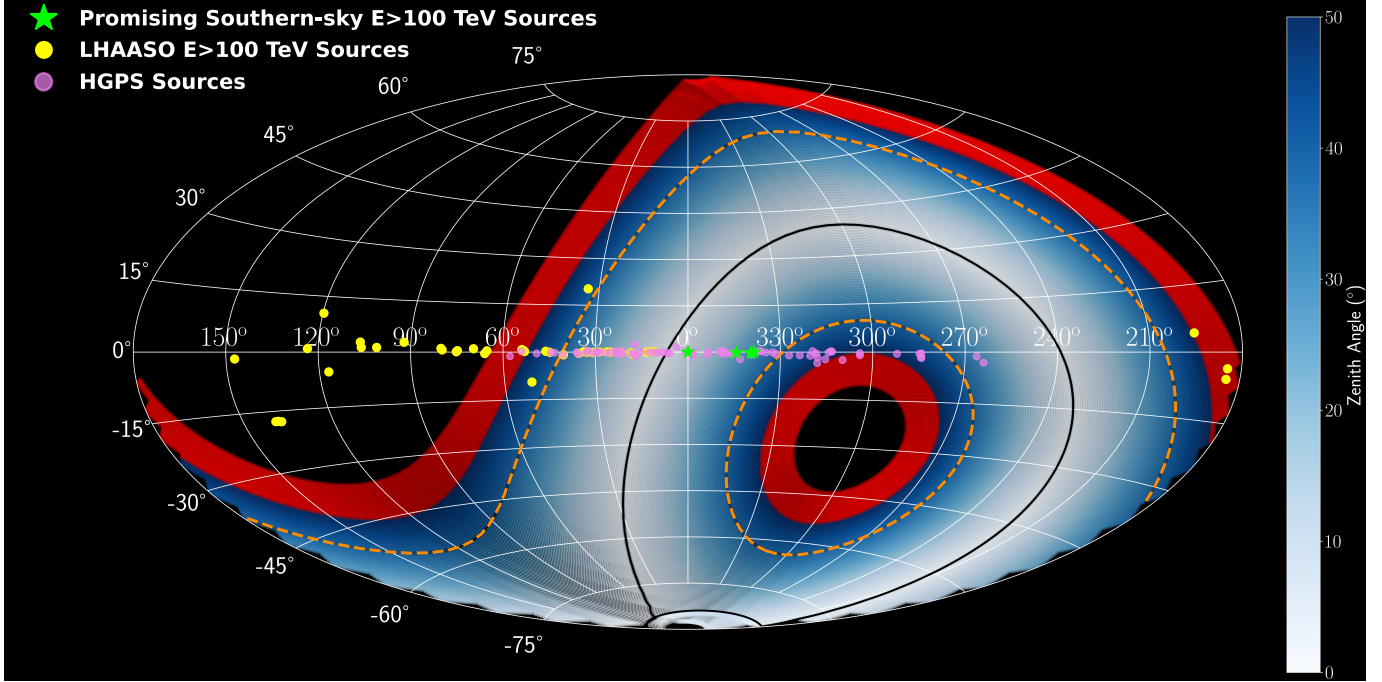


Figure 5: The SWGO visibility plot for the Southern-sky assuming the observatory situated at 23° South latitude, which is a similar latitude location of the H.E.S.S. experiment (Aharonian et al., 2006). The gradient of blue colors illustrates the visibility of objects at different observation zenith angles, while the red shaded areas indicate sky regions where the observation zenith angle is between 40° and 50° , which are generally considered as sub-optimal observation conditions for obtaining reliable data. The black solid and dashed orange lines correspond to the sky visibility at the zenith angles of 0° and 30° , respectively. The yellow and magenta dots highlighted on the plot mark the position of the LHAASO sources showing significant ($S_{\text{UHE}} \geq 4\sigma$) $E > 100$ TeV γ -ray emission regions (Cao et al., 2023b) and VHE sources detected in the H.E.S.S. Galactic Plane Survey (H. E. S. S. Collaboration et al., 2018), respectively. The green stars mark the location of promising $E > 100$ TeV Southern sky sources, namely the GC diffuse emission region, HESS J1702–420A, Westerlund 1 and HESS J1641–463, discussed extensively in Sec. 6. The plot is produced using the `swgo-plot` module provided in <https://swgo-collaboration.gitlab.io/swgo-plot/>.

ideal conditions, with zenith angles smaller than 30° , assuming the observatory being situated $\sim 23^\circ$ South latitudes. These promising candidates discussed in this section are presumed to be spatially isolated and are treated as point-like sources for SWGO. The assumption of a point-like source holds true for HESS J1702–420A and HESS J1641–463, since their spatial extensions of $0.06^\circ \pm 0.02^\circ$ (stat) $\pm 0.03^\circ$ (sys) (Abdalla, H. et al., 2021) and an upper limit of 0.05° (Abramowski et al., 2014a) degrees, respectively, are significantly smaller than SWGO’s design angular resolution of $\sim 0.15^\circ$ above 30 TeV. However, the GC diffuse emission region is defined with an outer radius of 0.45° (HESS Collaboration et al., 2016), and the emission region around Westerlund 1 extends up to a diameter of $\sim 2^\circ$ (Aharonian, F. et al., 2022), clearly deviating from the point-like source assumption for SWGO. Additionally, it’s important to note that all sources are actually not "spatially isolated" and they potentially suffer from the effects of source confusion, where the presence of multiple nearby γ -ray sources complicates the analysis in practice. We explicitly state that due to these idealized assumptions, the following estimates can only serve as first benchmarks within simplified conditions.

6.1. The GC diffuse emission region and the unidentified source HESS J1702–420A

The PTS analysis of the available VHE γ -ray data from the H.E.S.S. experiment for the GC diffuse emission and

HESS J1702–420A regions was presented and extensively discussed in Angüner et al. (2023), resulting in non-significant S_{PTS} values of 0.4σ and 1.0σ , respectively. Assuming $\xi = 20\%$ systematic error in the H.E.S.S. data sets, the corresponding 95% CL cutoff lower limits were calculated for the underlying hadronic spectra, yielding 172 TeV for the GC diffuse emission region and 436 TeV for HESS J1702–420A. Due to these results, it was not possible to draw any statistically significant conclusions regarding the PeVatron nature of these sources. However, it was discussed that the potential impact of forthcoming observatories, particularly the SWGO experiment, is crucial since both sources lack UHE data above 100 TeV, and data from such future observatories could provide crucial insights on determining whether these sources can be classified as Galactic PeVatrons.

6.2. Westerlund 1: The young massive stellar cluster

One of the regions in the Southern-sky showing potential promise for emitting UHE γ -rays above 100 TeV is the Westerlund 1 region, which stands out as the most massive young stellar cluster (YMC) within our Galaxy, estimated to be around 4–5 Myr old according to Clark, J. S. et al. (2005). The YMC environments in our Galaxy serve as fertile grounds for star formation, containing stars in the early stages of formation, surrounded by cosmic gas and dust. As a result of such conditions, these environments become efficient regions for accelerating particles which can interact with the surrounding gas, and are

Table 1: Spectral characteristics of the promising Southern-sky $E>100$ TeV γ -ray sources, the GC diffuse emission region (HESS Collaboration et al., 2016), HESS J1702–420A (Abdalla, H. et al., 2021), Westerlund 1 (Aharonian, F. et al., 2022) and HESS J1641–463 (Abramowski et al., 2014a). The differential flux at 1 TeV is provided in both $\text{TeV}^{-1}\text{cm}^{-1}\text{s}^{-1}$ and mCrab units in the second and third columns, while the corresponding differential flux at 10 TeV is given in the fourth column. Details regarding the best-fit γ -ray spectral indices, spectral cutoffs (if detected), and the favored γ -ray models are provided in the fifth, sixth, and seventh columns, respectively. We note that the $\Phi_0(1\text{ TeV})$ value of HESS J1702–420A is derived by extrapolating the γ -ray model described in Abdalla, H. et al. (2021) down to 1 TeV energy. The E_{Max} column gives the energy of the highest significant flux point, while the energy of the highest flux upper limits (if exists) are provided in parentheses.

Source	$\Phi_0(1\text{ TeV})$	$\Phi_0(1\text{ TeV})$	$\Phi_0(10\text{ TeV})$	Spectral	$E_{\text{cut},\gamma}$	Preferred	E_{Max}
Name	($\text{TeV}^{-1}\text{cm}^{-1}\text{s}^{-1}$)	(mCrab)	($\text{TeV}^{-1}\text{cm}^{-1}\text{s}^{-1}$)	Index	(TeV)	Model	(TeV)
GC diffuse emission	$(1.92\pm 0.08)\times 10^{-12}$	~ 50	$\sim 9.2\times 10^{-15}$	2.32 ± 0.05	–	PL	39.6 (58.8)
HESS J1702–420A	$\sim 1.6\times 10^{-13}$	~ 4	$\sim 4.7\times 10^{-15}$	1.53 ± 0.19	–	PL	84.8 (130.1)
Westerlund 1	$(1.00\pm 0.03)\times 10^{-11}$	~ 260	$\sim 4.0\times 10^{-14}$	2.30 ± 0.04	44^{+17}_{-11}	ECPL	80.6
HESS J1641–463	$(3.91\pm 0.69)\times 10^{-13}$	~ 10	$\sim 3.3\times 10^{-15}$	2.07 ± 0.11	–	PL	23.4 (68.7)

considered as promising Galactic PeVatron candidates (Morlino et al., 2021). A recent detailed VHE analysis of the region using H.E.S.S. data revealed the presence of an extended and complex shell-like γ -ray emission spanning up a diameter of $\sim 2^\circ$. The authors mentioned that even though there is not a clear spatial correlation between the structures of interstellar gas and the observed VHE γ -ray emission, the possibility of a scenario involving hadronic interactions is still possible due to the lack of energy-dependent morphology and uncertainties of the gas distribution (Aharonian, F. et al., 2022).

The ECPL model, given in Eq. 1, was fitted to the γ -ray flux data points of Westerlund 1, considering systematic errors of $\xi = 20\%$, resulting in $\Phi_0(1\text{ TeV})=(1.02\pm 0.07)\times 10^{-11}\text{ TeV}^{-1}\text{cm}^{-1}\text{s}^{-1}$, $\Gamma_\gamma=2.33\pm 0.08$ and $E_{\text{cut},\gamma}=44.2\pm 21.4\text{ TeV}$, which are consistent with the findings presented in Aharonian, F. et al. (2022). In this context, the statistical significance of the γ -ray spectral cutoff feature is found to be $S_{\text{cut},\gamma}=2.4\sigma$, and the corresponding lower limit for the γ -ray cutoff at the 95% CL is $LL_{\text{cut},\gamma}=23\text{ TeV}$. Assuming that the entire γ -ray emission arises from interactions between accelerated protons, following the spectral shape defined in Eq. 2, and target gas in the region, the spectral index and cutoff parameters of the underlying parental proton spectral can be obtained as $\Gamma_p=2.33\pm 0.12$ and $E_{\text{cut},p}=300\pm 188\text{ TeV}$, respectively. The statistical significance of the proton cutoff feature is calculated as $S_{\text{cut},p}=2.4\sigma$, while the 95% CL lower limit for the proton cutoff is derived at 127 TeV. The corresponding PTS significance for the overall emission originating from the Westerlund 1 region is estimated to be $S_{\text{PTS}}=-1.4\sigma$. When considering only the available H.E.S.S. data, a conclusive determination cannot be made regarding whether the emission from Westerlund 1 arises from PeVatron activity. Consequently, further observations at UHE, particularly above 100 TeV, are crucial to reach a conclusive determination of the PeVatron nature of Westerlund 1.

6.3. The unidentified source HESS J1641–463

The unidentified source HESS J1641–463 in the Southern-sky presents another promising region for the emission of $E>100$ TeV γ -rays. The source exhibits a hard VHE γ -ray spectrum extending up to a few tens of TeV without showing any

significant spectral cutoff (Abramowski et al., 2014a; Angüner et al., 2018). Similar to the situation with HESS J1702–420A, the source is affected by source confusion due to the presence of the bright and extended ($\sim 0.11^\circ$) γ -ray source HESS J1640–465 (Abramowski et al., 2014b), which is located $\sim 0.28^\circ$ away and showing a significant γ -ray cutoff in its spectrum at $\sim 6\text{ TeV}$. There are dense molecular clouds found toward the line of sight, along with two nearby supernova remnants, SNR G338.3–0.0 and SNR G338.5+0, while the latter is found to be spatially coincident with the source. These neighboring SNRs could potentially serve as sources of accelerated protons, suggesting a plausible hadronic scenario for the observed emission. By using the γ -ray flux data points from HESS J1641–463 and assuming a $\xi = 20\%$ systematic error, lower limits for the γ -ray spectral cutoff at a 95% CL are derived as $LL_{\text{cut},\gamma}=12.4\text{ TeV}$. Under the hypothesis that the entire γ -ray emissions originates from a hadronic interactions, the spectral index of the parent protons and the 95% CL lower limit for the proton cutoff parameters can be determined as $\Gamma_p=2.03\pm 0.15$ and $LL_{\text{cut},p}=64.1\text{ TeV}$, respectively, while the significance of the PTS is found to be $S_{\text{PTS}}=0.6\sigma$. Similarly to the Westerlund 1 case, robust conclusions on the PeVatron nature of HESS J1641–463 cannot be drawn when taking into account only the H.E.S.S. data, emphasizing the need for additional UHE data to provide further insights.

6.4. SWGO simulations and data analysis of the promising Southern-sky PeVatron candidates

For all the sources discussed in this section, the available spectral H.E.S.S. data assuming a minimum relative flux error of $\xi = 20\%$ are fitted to the hadronic emission model defined by Eq. 2. The resulting best-fit hadronic models obtained from the analysis of H.E.S.S. data are adjusted and further used in the SWGO simulations of each individual source under investigation. An example simulation result of 5 years SWGO observations is shown in Fig. 6 for the diffuse emission region in the vicinity of the GC (top left panel), the unidentified γ -ray source HESS J1702–420A (top right panel), Westerlund 1 region (bottom left panel) and HESS J1641–463 (bottom right panel). The solid lines in Fig. 6 represent the hadronic models

reconstructed from H.E.S.S. data with an energy cutoff fixed at 3 PeV. These hypothetical PeVatron models correspond to the expected γ -ray emission from Galactic PeVatrons, which can significantly contribute to the knee structure observed in the CR spectrum. On the other hand, the dashed lines in the figure represent best-fit non-PeVatron models derived from the same H.E.S.S. data. For these non-PeVatron models, the hadronic energy cutoff is fixed to the derived 95% CL lower limit of the underlying proton spectral cutoff obtained from respective H.E.S.S. observations: 172 TeV for the GC diffuse emission region, 436 TeV for HESS J1702–420A, 127 TeV for Westerlund 1, and 64 TeV for HESS J1641–463. These non-PeVatron models, characterized by proton cutoff energies fixed at their respective 95% CL lower limits, remain significantly below 3 PeV, consequently are not expected to substantially contribute to the knee feature. To assess the impact of systematic errors, the SWGO flux data for PeVatron and non-PeVatron models are simulated considering statistical errors only ($\xi = 0$), and with an additional optimistic $\xi = 5\%$ and conservative $\xi = 10\%$ systematic errors. The red SWGO flux data points shown in Fig. 6 account only for statistical errors ($\xi = 0$).

In order to accumulate reliable statistics, the simulation procedure described above is repeated 500 times for all examined sources, and S_{PTS} values are calculated assuming PeVatron and non-PeVatron models considering systematic errors of $\xi = 0$, $\xi = 5\%$ and $\xi = 10\%$ in each simulated SWGO data set. In addition, the best fit proton and γ -ray spectral cutoff energies ($E_{cut,p}$ and $E_{cut,\gamma}$), statistical significance of the respective proton and γ -ray cutoff features ($S_{cut,p}$ and $S_{cut,\gamma}$) and the 95% CL of proton and γ -ray spectral cutoff lower limits ($LL_{cut,p}$ and $LL_{cut,\gamma}$) are derived for each simulated SWGO data set. These characteristics derived from 500 simulations are then gathered into distributions, and their median values along with standard errors are computed and summarized in Table 2.

The derived intrinsic properties mentioned above have the potential to provide insights about the PeVatron characteristics of sources. The results of the simulations clearly indicate that if the examined γ -ray sources are associated to hadronic Galactic PeVatrons, which contribute to the knee feature observed at 3 PeV energies, SWGO possesses substantial potential to confirm their PeVatron nature at a robust CL ($S_{PTS} \geq 5.0\sigma$). Similarly, the absence of PeVatron characteristics can also be robustly confirmed ($S_{PTS} \leq -5.0\sigma$) for all sources, provided that the corresponding proton energy cutoffs are well below 3 PeV. Given the specific cutoff values assigned to the assumed respective proton spectra, the application of the PTS technique using spectral data inferred from SWGO observations allow a robust determination of whether the γ -ray emissions from these promising Southern-sky $E > 100$ TeV sources are Galactic PeVatrons in nature.

When a conservative $\xi = 10\%$ SWGO systematic error is considered alongside with otherwise unchanged simulation parameters, the median significances of the PTS values are diminished to a marginal detection range of $S_{PTS} \cong 3-4\sigma$ for PeVatron cases, while the instances where non-PeVatron characteristics can still be robustly confirmed, with the exception of HESS J1702–420A. On the other hand, in the case of $\xi = 5\%$ SWGO systematic error, robust detection of both PeVatron and

non-PeVatron characteristics can be confirmed. These simulation results clearly highlight the importance of inferred systematics, and show that the full potential of SWGO in PeVatron searches can only be achieved when systematic errors are carefully controlled and minimized as effectively as possible. Especially, systematic flux error levels similar to LHAASO experiment or better ($\xi = 5-7\%$) can lead to significant detection of spectral PeVatron characteristics. Furthermore, assuming point-like source morphology for the extended GC diffuse emission and Westerlund 1 regions can have significant impact on the results. As it was shown in (Acero, F. et al., 2023), both the PeVatron detection and rejection probabilities decrease as the source extension increases (see Ambrogi et al. (2018) for a detailed discussion on extended source sensitivities). Consequently, the S_{PTS} values (and lower limits, $LL_{cut,p}$, $LL_{cut,\gamma}$) obtained for these extended sources tend to be overestimated.

7. Discussions and Conclusions

In practical applications, it is expected that the issue of source confusion, which refers to the condition where multiple γ -ray sources exist within an unresolved spatial distance, becomes a significant challenge when analysing Galactic γ -ray data. This challenge is particularly pronounced when dealing with γ -ray energies below 10 TeV, given that many Galactic VHE sources are known either to exhibit cutoffs in their spectra below these energies, or not to emit significant flux above 10 TeV due to soft power-law spectral index of the emission. As a result, the problem of source confusion becomes more relevant with decreasing γ -ray energy. One particular example is the unidentified source HESS J1702–420 discussed in this paper. The investigation of data from HESS J1702–420 has revealed two closely positioned sub-components without the detection of significant energy cutoff (Abdalla, H. et al., 2021). In this particular case, the component HESS J1702–420A becomes more luminous than the second component, HESS J1702–420B, above a few tens of TeV due to relative difference in their power-law spectral indices. Another example comes from the observations of a specific Galactic region encompassing the Boomerang PWN and SNR G106.3+2.7. The observations of this region conducted by MAGIC provided compelling evidence that supports the existence of two distinct power-law source components (MAGIC Collaboration et al., 2023). The softer of the two components, referred to as the ‘head’, and the harder one, known as the ‘tail’, both show no clear spectral cutoffs. Moreover, the observations carried out by LHAASO in the same region (Cao and others, 2021) exclusively detect a single source component emitting at UHEs, and as it was discussed in Angüner et al. (2023), the UHE emission detected by LHAASO can be connected to the tail emission detected by MAGIC. In contrary, when examining the case of HESS J1641–463, which exhibits a hard power-law spectrum, the neighboring source HESS J1640–465 shows a significant spectral cutoff in its spectrum below 10 TeV. These examples show that γ -ray emission beyond several tens of TeV can be well dominated by a single source even in the case of source confusion, particularly either when no spectral cutoff

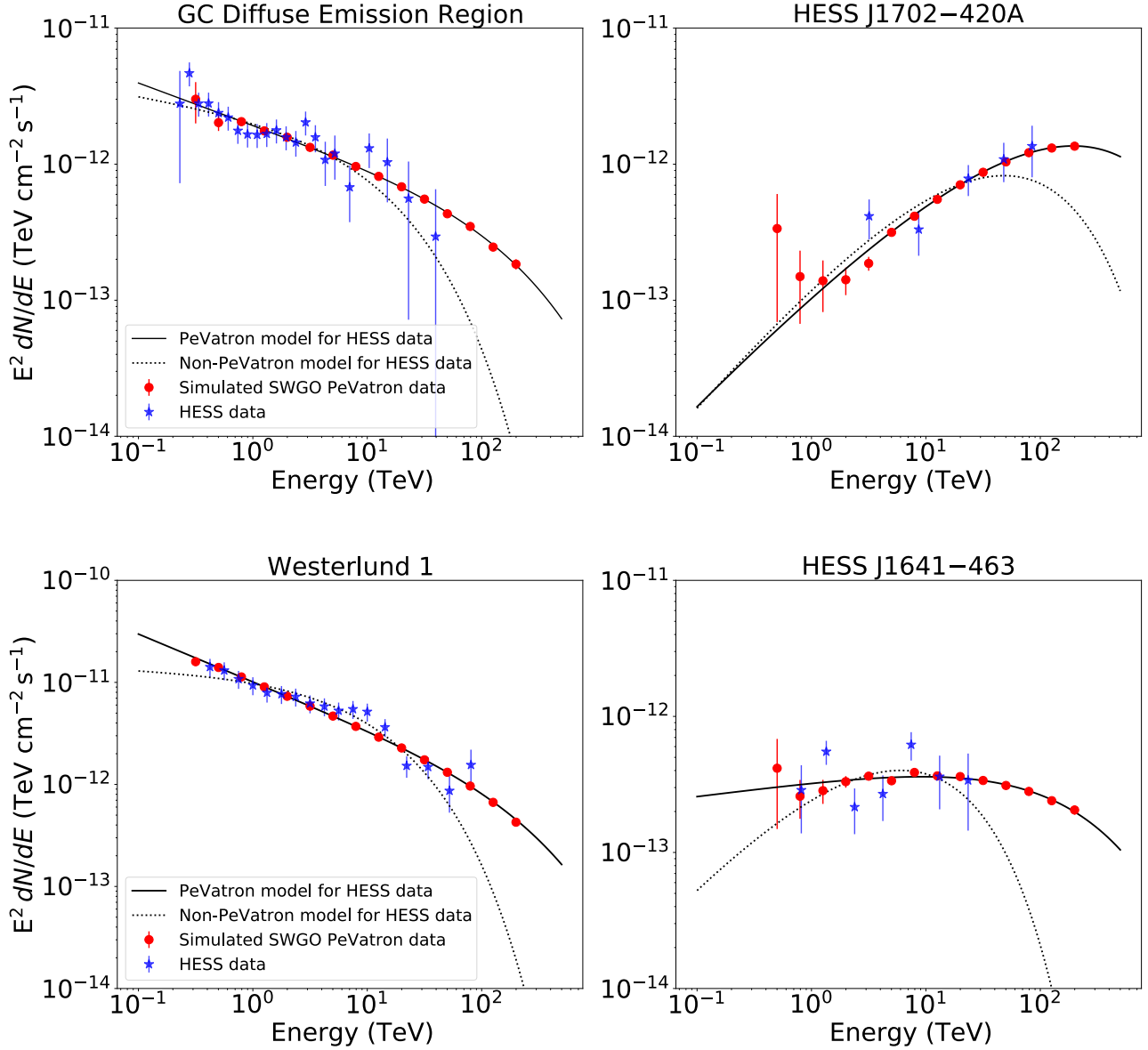


Figure 6: Simulated γ -ray spectra from 5 years of SWGO data for the GC diffuse emission region (upper left panel), HESS J1702-420A (upper right panel), Westerlund 1 (lower left panel) and HESS J1641-463 (lower right panel). The 5-year straw-man configuration sensitivity of SWGO taken from <https://github.com/harmscho/SGSOSensitivity> is used in simulations. Spectral γ -ray flux data from observations with H.E.S.S. are shown in blue stars with an assumed minimal relative flux error of $\xi = 20\%$. Solid black lines show the best fit PeVatron models with a hadronic energy cutoff fixed at 3 PeV, while the dashed black lines are the best-fit non-PeVatron models in which hadronic energy cutoffs are fixed the respective 95% CL lower limit derived from the H.E.S.S. data. The SWGO flux points obtained from the simulation of the best fit PeVatron models are shown in red without considering any systematic errors ($\xi = 0\%$).

is detected or the spectral index of one component is significantly harder than for the neighboring sources. Consequently, an unprecedented level of information on comprehensive understanding of the PeVatron nature of sources can be acquired from the synergy between the experiments like CTA and SWGO due to their complementary capabilities, with CTA excelling in superior angular resolution and SWGO enhancing flux sensitivity at high energies.

As evident from both Fig. 1 and Fig. 2, the flux sensitivity of SWGO will offer a simple detection γ -ray sources at high ener-

gies, providing an unprecedented level of statistical information beyond 10 TeV, at which concerns related to source confusion is effectively eliminated. On the other hand, the superior angular resolution of CTA will provide crucial information for resolving individual sources below a few tens of TeV energies, at which source confusion is expected to have more significant impact, and therefore supplying key insights into the source component with which the observed UHE emission can be associated. Such a clear association between a γ -ray source exhibiting distinct PeVatron spectral signatures and any type of Galactic CR

Table 2: Analysis results inferred from the SWGO simulations of four promising Southern-sky $E > 100$ TeV sources. Each source instance is simulated 500 times and the results are obtained from the respective distributions of derived properties. The ‘PeV’ and ‘Non-PeV’ identifiers next to source names indicate whether the PeVatron ($E_{\text{cut,p}}$ fixed to 3 PeV) or Non-PeVatron ($E_{\text{cut,p}}$ fixed to derived 95% proton cutoff lower limits) hadronic models used when simulating the SWGO flux data, while ξ is the assumed minimal relative flux error explained in Sec. 3. S_{PTS} and $LL_{\text{cut,p}}$ denote the significance of the PTS and the 95% CL lower limit on the hadronic energy cutoff $E_{\text{cut,p}}$, while $S_{\text{cut,p}}$ is the significance of the hadronic cutoff feature, respectively. Similarly, $LL_{\text{cut,\gamma}}$ and $S_{\text{cut,\gamma}}$ are the corresponding 95% CL lower limit on the γ -ray cutoff energy $E_{\text{cut,p}}$ and the significance of the γ -ray cutoff feature. The derived reference properties, on which conclusions are based in this work, are highlighted in bold and shown in Fig. 6.

Source Name	ξ (%)	S_{PTS} (σ)	$LL_{\text{cut,p}}$ (TeV)	$S_{\text{cut,p}}$ (σ)	$E_{\text{cut,p}}$ (TeV)	$LL_{\text{cut,\gamma}}$ (TeV)	$S_{\text{cut,\gamma}}$ (σ)	$E_{\text{cut,\gamma}}$ (TeV)
GC diffuse emission (PeV)	0	11.7±1.0	2479±285	11.9±1.0	3020±391	244±21	11.5±1.0	282±28
GC diffuse emission (PeV)	5	6.6±0.7	2153±314	6.6±0.8	3022±545	240±27	6.4±0.8	307±43
GC diffuse emission (PeV)	10	4.1±0.6	1795±312	4.2±0.7	2969±759	220±26	4.1±0.8	316±58
GC diffuse emission (Non-PeV)	0	-22.4±1.0	158±9	33.8±1.1	173±10	33±1	33.6±1.1	36±1
GC diffuse emission (Non-PeV)	5	-12.8±0.7	148±9	18.8±0.7	172±11	34±2	18.6±0.7	37±2
GC diffuse emission (Non-PeV)	10	-8.6±0.7	139±13	12.3±0.7	173±17	34±3	12.1±0.7	40±3
HESS J1702–420A (PeV)	0	19.8±1.2	2593±243	25.2±0.9	3053±290	271±10	25.0±0.9	290±12
HESS J1702–420A (PeV)	5	4.3±0.3	1773±329	7.2±0.5	3021±592	201±11	7.3±0.4	248±19
HESS J1702–420A (PeV)	10	2.3±0.3	1250±332	4.1±0.5	3100±1012	166±12	4.2±0.4	236±24
HESS J1702–420A (Non-PeV)	0	-11.0±1.0	427±7	45.5±1.0	441±21	102±3	44.0±1.0	107±3
HESS J1702–420A (Non-PeV)	5	-4.9±0.7	415±9	18.2±0.7	449±32	97±3	17.7±0.7	107±4
HESS J1702–420A (Non-PeV)	10	-2.8±0.5	397±10	10.2±0.5	453±48	86±4	10.0±0.4	102±5
Westerlund 1 (PeV)	0	37.5±1.0	2805±109	34.6±1.0	2996±121	279±8	34.3±1.0	294±9
Westerlund 1 (PeV)	5	8.5±0.5	2290±198	8.1±0.7	2899±313	281±18	7.9±0.7	344±27
Westerlund 1 (PeV)	10	4.3±0.2	1832±126	4.1±0.3	2999±296	237±12	4.0±0.3	342±26
Westerlund 1 (Non-PeV)	0	-141.3±1.0	126±1	197.7±1.3	128±1	28±1	196.5±1.3	29±1
Westerlund 1 (Non-PeV)	5	-26.5±0.6	118±3	34.8±0.7	128±4	31±1	34.3±0.8	33±1
Westerlund 1 (Non-PeV)	10	-16.2±0.6	113±6	20.5±0.6	128±7	32±2	20.1±0.6	36±2
HESS J1641–463 (PeV)	0	6.7±1.0	2225±398	8.9±0.1	3050±625	219±25	8.3±1.0	268±37
HESS J1641–463 (PeV)	5	5.2±0.8	2032±392	6.5±0.8	3045±717	211±25	6.1±0.8	273±41
HESS J1641–463 (PeV)	10	3.6±0.6	1721±368	4.3±0.7	3065±930	191±23	4.0±0.7	275±50
HESS J1641–463 (Non-PeV)	0	-18.5±1.0	56±4	24.7±1.1	65±7	21±1	24.5±1.2	23±1
HESS J1641–463 (Non-PeV)	5	-14.8±0.9	55±4	19.2±0.9	65±8	21±2	19.1±0.9	23±2
HESS J1641–463 (Non-PeV)	10	-10.0±0.7	54±4	12.9±0.7	66±10	20±2	12.7±0.7	23±3

accelerator is essential for robust determination of Galactic objects which are truly the PeVatrons responsible for the knee feature observed in the CR spectrum. As a result, such a synergy can potentially shed light on the century-old enigma of the origin of Galactic CRs. However, when addressing the issue of source confusion through a combined analysis of data from different observatories, such as future CTA South and SWGO, the relative systematic errors between the flux measurements of different observatories must be carefully controlled.

In this paper, the expected potential of SWGO in PeVatron searches are investigated using the straw-man design sensitivity curve. It was concluded that the high energy γ -ray cutoffs between 30 TeV and 100 TeV can be significantly detected for relatively faint 5 mCrab sources, when the spectral index is hard ($\Gamma \lesssim 2.0$), while the detection of spectral cutoffs for the relatively soft $\Gamma \approx 2.3$ sources can only be possible if they are bright enough, i.e. $\Phi_0 \geq 11$ mCrab. The reconstructed SWGO PeVatron detection maps show that the SWGO can probe large

parts of the investigated PeVatron parameter space, providing a robust detection and/or rejection power. A dedicated study on the promising Southern-sky $E > 100$ TeV sources gives similar results, concluding that the SWGO will have a great potential to confirm or exclude their PeVatron nature at a robust significance level after 5-years of observation. The study also demonstrates that the control of SWGO systematic errors will be a necessary issue, and they should be around 5 – 7% in order to reach the maximized potential of detecting spectral PeVatron characteristics. We explicitly mention that the results presented in this paper do not reflect a fiducial performance of the planned SWGO observatory, instead can provide a preliminary insight on the performance of PeVatron searches with SWGO. The results presented in this paper are based on straw-man design configuration, therefore they are conservative. Indeed, with the low and high energy enhancements, together with improved PSF and background rejection, the performance capabilities, especially SWGO abilities to detect spectral cutoffs at high energies and PeVatron signatures will be significantly improved.

LHAASO: Large High Altitude Air Shower Observatory
LL: Lower Limit
MAGIC: Major Atmospheric Gamma-Ray Imaging Cherenkov
MC: Monte-Carlo
PL: Power-Law
PSF: Point Spread Function
PTS: PeVatron Test Statistics
SN: Supernova
SNR: Supernova Remnant
SWGO: Southern Wide-field Gamma-ray Observatory
TS: Test Statistics
UHE: Ultra High Energy
VHE: Very High Energy
WCD: Water Cherenkov Detector
YMC: Young Massive stellar Cluster

Acknowledgements

E.O.A. acknowledges financial support by TÜBİTAK Research Institute for Fundamental Sciences. We express our sincere gratitude to Gerrit Spengler for his extremely useful active contributions and constructive feedback. We also express our sincere gratitude to the SWGO Collaboration, especially the feedbacks provided by Ulisses Barres, Ruben Conceição and Sidharth Sreeja Sadanandan, which greatly enhanced the quality of the paper.

Appendix A. Parameter scan at 1 TeV flux normalization

The PeVatron detection and rejection maps provided in Sec. 5 uses the flux normalization of sources at 10 TeV, which is much more suited for WCD experiments that have enhanced high energy flux sensitivity. In order to connect these maps to current and future VHE experiments which in general have their maximized flux sensitivity at 1 TeV, the maps reconstructed using Φ_0 at 1 TeV are also provided in this appendix in Fig. A.7.

List of Acronyms

CL: Confidence Level
CR: Cosmic Ray
CTA: Cherenkov Telescope Array
EAS: Extensive Air Shower
ECPL: Power-Law with Exponential Cutoff
FoV: Field of View
GC: Galactic Center
H.E.S.S.: High Energy Stereoscopic System
HAWC: High Altitude Water Cherenkov Observatory
HE: High Energy
IACs: Imaging Atmospheric Cherenkov Telescopes
IRF: Instrument Response Function

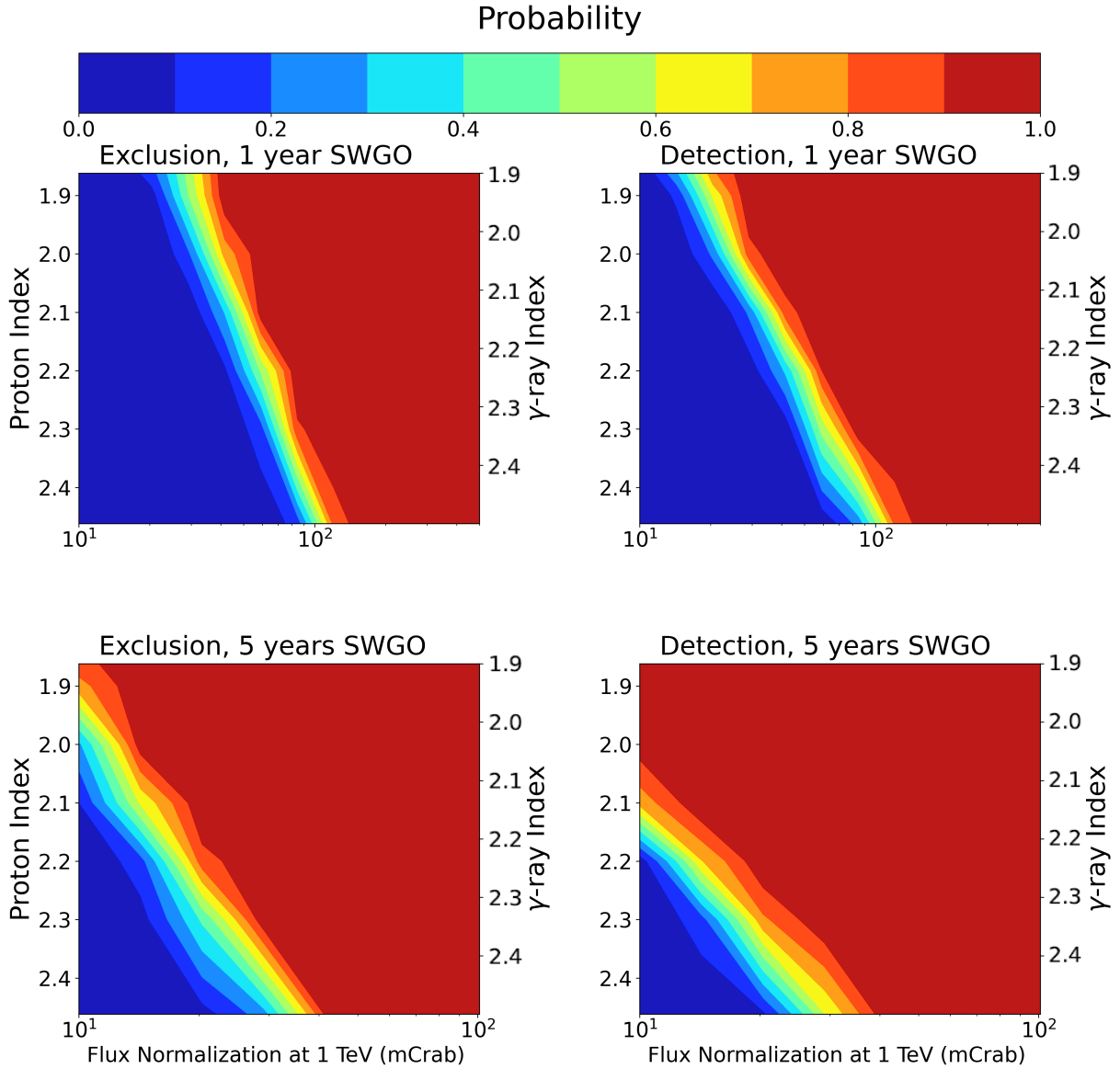


Figure A.7: Estimated probability for exclusion and detection of a PeVatron association at a respective statistical significance of 5σ with SWGO data assuming the straw-man (Albert, A. et al., 2019) SWGO sensitivity taken from <https://github.com/harmscho/SGSOSensitivity>. The abscissa, left and right ordinate show the assumed parameters for the true observed γ -ray flux normalization Φ_0 at 1 TeV originating from pp interactions observed from Earth, the spectral index of the hadronic particle population Γ_p and the corresponding spectral index of ECPL γ -ray emission. The color bar indicates the probability to exclude (left panels) and detect (right panels) a PeVatron with a statistical significance of 5σ with the PTS. One year of SWGO observations is shown in the upper panels, while 5 years of SWGO observations are shown in the lower panels. The assumed hadronic cutoff energy for the left panels, which show the exclusion power at a significance of 5σ , is $E_{\text{cut},p}=400$ TeV. On the other hand, $E_{\text{cut},p}=3$ PeV is used for the right panels, which show the respective SWGO PeVatron detection power.

References

- Abbasi, R., et al., 2009. The IceCube data acquisition system: Signal capture, digitization, and timestamping. *Nucl. Instrum. Methods Phys. Res. A* 601, 294–316. doi:10.1016/j.nima.2009.01.001, arXiv:0810.4930.
- Abbasi, R., et al. (IceCube), 2023. Observation of high-energy neutrinos from the Galactic plane. *Science* 380, adc9818. doi:10.1126/science.adc9818, arXiv:2307.04427.
- Abdalla, H. et al., 2021. Evidence of 100 TeV emission from HESS J1702-420: A new PeVatron candidate. *A&A* 653, A152. URL: <https://doi.org/10.1051/0004-6361/202140962>, doi:10.1051/0004-6361/202140962.
- Abe, S., et al. (CTA Consortium), 2023. Prospects for a survey of the Galactic plane with the Cherenkov Telescope Array arXiv:2310.02828.
- Abeysekara, A.U., et al. (HAWC), 2018. Very high energy particle acceleration powered by the jets of the microquasar SS 433. *Nature* 562, 82–85. doi:10.1038/s41586-018-0565-5. [Erratum: *Nature* 564, E38 (2018)].
- Abeysekara, A.U., et al. (HAWC Collaboration), 2020. Multiple Galactic Sources with Emission Above 56 TeV Detected by HAWC. *Phys.*

- Rev. Lett. 124, 021102. URL: <https://link.aps.org/doi/10.1103/PhysRevLett.124.021102>, doi:10.1103/PhysRevLett.124.021102.
- Abeyskara, A.U. et al., 2017. Observation of the Crab Nebula with the HAWC Gamma-Ray Observatory. *The Astrophysical Journal* 843, 39. URL: <https://dx.doi.org/10.3847/1538-4357/aa7555>, doi:10.3847/1538-4357/aa7555.
- Abramowski et al., 2014a. Discovery of the Hard Spectrum VHE γ -Ray Source HESS J1641-463. *ApJ letters* 794, L1. doi:10.1088/2041-8205/794/1/L1, arXiv:1408.5280.
- Abramowski et al., 2014b. HESS J1640-465 - an exceptionally luminous TeV γ -ray supernova remnant. *MNRAS* 439, 2828–2836. doi:10.1093/mnras/stu139.
- Acero, F. et al., 2023. Sensitivity of the Cherenkov Telescope Array to spectral signatures of hadronic PeVatrons with application to Galactic Supernova Remnants. *Astroparticle Physics* 150, 102850. URL: <https://www.sciencedirect.com/science/article/pii/S0927650523000361>, doi:<https://doi.org/10.1016/j.astropartphys.2023.102850>.
- Acharya, B., et al., 2013. Introducing the CTA concept. *Aph* 43, 3–18. doi:10.1016/j.astropartphys.2013.01.007.
- Ackermann, M., 2013. Detection of the Characteristic Pion-Decay Signature in Supernova Remnants. *Science* 339, 807. doi:10.1126/science.1231160.
- Ackermann, M., et al., 2011. A cocoon of freshly accelerated cosmic rays detected by fermi in the cygnus superbubble. *Science* 334, 1103–1107. URL: <https://www.science.org/doi/abs/10.1126/science.1210311>, doi:10.1126/science.1210311, arXiv:<https://www.science.org/doi/pdf/10.1126/science.1210311>.
- Adriani, O., CALET Collaboration, 2022. Observation of Spectral Structures in the Flux of Cosmic-Ray Protons from 50 GeV to 60 TeV with the Calorimetric Electron Telescope on the International Space Station. *Phys. Rev. Lett.* 129, 101102. doi:10.1103/PhysRevLett.129.101102.
- Adriani, O., et al., 2011. PAMELA Measurements of Cosmic-Ray Proton and Helium Spectra. *Science* 332, 69–72. URL: <https://www.science.org/doi/abs/10.1126/science.1199172>, doi:10.1126/science.1199172, arXiv:<https://www.science.org/doi/pdf/10.1126/science.1199172>.
- Aguilar, M., et al. (AMS Collaboration), 2015a. Precision Measurement of the Helium Flux in Primary Cosmic Rays of Rigidities 1.9 GV to 3 TV with the Alpha Magnetic Spectrometer on the International Space Station. *Phys. Rev. Lett.* 115, 211101. URL: <https://link.aps.org/doi/10.1103/PhysRevLett.115.211101>, doi:10.1103/PhysRevLett.115.211101.
- Aguilar, M., et al. (AMS Collaboration), 2015b. Precision Measurement of the Proton Flux in Primary Cosmic Rays from Rigidity 1 GV to 1.8 TV with the Alpha Magnetic Spectrometer on the International Space Station. *Phys. Rev. Lett.* 114, 171103. URL: <https://link.aps.org/doi/10.1103/PhysRevLett.114.171103>, doi:10.1103/PhysRevLett.114.171103.
- Aharonian, F., Yang, R., de Oña Wilhelmi, E., 2019. Massive stars as major factories of Galactic cosmic rays. *Nature Astronomy* 3, 561–567. doi:10.1038/s41550-019-0724-0, arXiv:1804.02331.
- Aharonian, F., et al., 2021. Observation of the crab nebula with lhaaso-km2a - a performance study. *Chinese Physics C* 45, 025002. URL: <https://dx.doi.org/10.1088/1674-1137/abd01b>, doi:10.1088/1674-1137/abd01b.
- Aharonian et al., 2006. Observations of the Crab nebula with HESS. *A&A* 457, 899–915. URL: <https://doi.org/10.1051/0004-6361/20065351>, doi:10.1051/0004-6361/20065351.
- Aharonian, F. et al., 2022. A deep spectromorphological study of the emission surrounding the young massive stellar cluster Westerlund 1. *A&A* 666, A124. URL: <https://doi.org/10.1051/0004-6361/202244323>, doi:10.1051/0004-6361/202244323.
- Ajello, M., et al., 2021. Fermi large area telescope performance after 10 years of operation. *The Astrophysical Journal Supplement Series* 256, 12. URL: <https://dx.doi.org/10.3847/1538-4365/ac0ceb>, doi:10.3847/1538-4365/ac0ceb.
- Albert, A. et al., 2019. Science Case for a Wide Field-of-View Very-High-Energy Gamma-Ray Observatory in the Southern Hemisphere. arXiv e-prints, arXiv:1902.08429 arXiv:1902.08429.
- Amato, E., 2014. The origin of galactic cosmic rays. *International Journal of Modern Physics D* 23, 1430013. doi:10.1142/S0218271814300134, arXiv:1406.7714.
- Amato, E., Blasi, P., 2018. Cosmic ray transport in the Galaxy: A review. *Advances in Space Research* 62, 2731–2749. doi:10.1016/j.asr.2017.04.019, arXiv:1704.05696.
- Amato, E., Casanova, S., 2021. On particle acceleration and transport in plasmas in the Galaxy: theory and observations. *Journal of Plasma Physics* 87, 845870101. doi:10.1017/S0022377821000064, arXiv:2104.12428.
- Amato, E., Olmi, B., 2021. The Crab Pulsar and Nebula as Seen in Gamma-Rays. *Universe* 7. doi:10.3390/universe7110448.
- Amato, E., Olmi, B., 2021. The Crab Pulsar and Nebula as Seen in Gamma-Rays. *Universe* 7, 448. doi:10.3390/universe7110448, arXiv:2111.07712.
- Amato, E., Guetta, D., Blasi, P., 2003. Signatures of high energy protons in pulsar winds. *A&A* 402, 827–836. doi:10.1051/0004-6361:20030279.
- Ambrogio, L., Celli, S., Aharonian, F., 2018. On the potential of cherenkov telescope arrays and km³ neutrino telescopes for the detection of extended sources. *Astroparticle Physics* 100, 69–79. URL: <https://www.sciencedirect.com/science/article/pii/S0927650517302931>, doi:<https://doi.org/10.1016/j.astropartphys.2018.03.001>.
- Amenomori, M., et al. (Tibet AS-gamma Collaboration), 2019. First Detection of Photons with Energy beyond 100 TeV from an Astrophysical Source. *Phys. Rev. Lett.* 123, 051101. URL: <https://link.aps.org/doi/10.1103/PhysRevLett.123.051101>, doi:10.1103/PhysRevLett.123.051101.
- Amenomori, M., et al. (Tibet AS-gamma Collaboration), 2021a. First Detection of sub-PeV Diffuse Gamma Rays from the Galactic Disk: Evidence for Ubiquitous Galactic Cosmic Rays beyond PeV Energies. *Phys. Rev. Lett.* 126, 141101. URL: <https://link.aps.org/doi/10.1103/PhysRevLett.126.141101>, doi:10.1103/PhysRevLett.126.141101.
- Amenomori, M., et al. (Tibet AS γ), 2021b. Potential PeVatron supernova remnant G106.3+2.7 seen in the highest-energy gamma rays. *Nature Astronomy* 5, 460–464. doi:10.1038/s41550-020-01294-9, arXiv:2109.02898.
- Anchordoqui, L.A., Barger, V., Cholis, I., Goldberg, H., Hooper, D., Kusenko, A., Learned, J.G., Marfatia, D., Pakvasa, S., Paul, T.C., Weiler, T.J., 2014. Cosmic neutrino pevatrons: A brand new pathway to astronomy, astrophysics, and particle physics. *Journal of High Energy Astrophysics* 1-2, 1–30. URL: <https://www.sciencedirect.com/science/article/pii/S2214400814000020>, doi:<https://doi.org/10.1016/j.jheap.2014.01.001>.
- Angüner, E.O., 2023. Exploring the high energy frontiers of the Milky Way with ground-based gamma-ray astronomy: PeVatrons and the quest for the origin of Galactic cosmic-rays. *Turkish Journal of Physics* 47. doi:<https://doi.org/10.55730/1300-0101.2738>.
- Angüner, E.O., Casanova, S., Oya, I., Aharonian, F., Bordas, P., Ziegler, A. (H.E.S.S.), 2018. Very high energy emission from the hard spectrum sources HESS J1641-463, HESS J1741-302 and HESS J1826-130. *PoS ICRC2017*, 686. doi:10.22323/1.301.0686.
- Angüner, E.O., Spengler, G., Amato, E., Casanova, S., 2023. Search for the Galactic accelerators of cosmic rays up to the knee with the Pevatron test statistic. *MNRAS* 523, 4097–4112. URL: <https://doi.org/10.1093/mnras/stad1674>, doi:10.1093/mnras/stad1674.
- ARGO-YBJ Collaboration, Bartoli, B., et al., 2015. Knee of the cosmic hydrogen and helium spectrum below 1 PeV measured by ARGO-YBJ and a Cherenkov telescope of LHAASO. *Phys. Rev. D* 92, 092005. doi:10.1103/PhysRevD.92.092005.
- Barres de Almeida, U., SWGO Collaboration, 2022. Benchmarking the Science for the Southern Wide-Field Gamma-ray Observatory (SWGO), in: 37th International Cosmic Ray Conference (ICRC2021). 12-13 July 2021. Berlin, p. PoS(ICRC2021)893.
- Bell, A.R., 1978. The acceleration of cosmic rays in shock fronts - I. *MNRAS* 182, 147–156. doi:10.1093/mnras/182.2.147.
- Bell et al., 2013. Cosmic-ray acceleration and escape from supernova remnants. *MNRAS* 431, 415–429. doi:10.1093/mnras/stt179.
- Binns et al., 2005. Cosmic-Ray Neon, Wolf-Rayet Stars, and the Superbubble Origin of Galactic Cosmic Rays. *ApJ* 634, 351–364. doi:10.1086/496959.
- Blasi, P., 2013. The origin of galactic cosmic rays. *A&A Reviews* 21, 70. doi:10.1007/s00159-013-0070-7, arXiv:1311.7346.
- Bykov, A.M., Marcowith, A., Amato, E., Kalyashova, M.E., Kruijssen, J.M.D., Waxman, E., 2020. High-Energy Particles and Radiation in Star-Forming Regions. *Space Science Reviews* 216, 42. doi:10.1007/s11214-020-00663-0.
- Cao, Z., others, 2021. Ultrahigh-energy photons up to 1.4 petaelectronvolts from 12 γ -ray Galactic sources. *Nature* 594, 33–36. doi:10.1038/s41586-021-03498-z.
- Cao, Z., et al. (LHAASO), 2023a. Measurement of ultra-high-energy dif-

- fuse gamma-ray emission of the Galactic plane from 10 TeV to 1 PeV with LHAASO-KM2A arXiv:2305.05372.
- Cao, Z., et al. (LHAASO), 2023b. The First LHAASO Catalog of Gamma-Ray Sources arXiv:2305.17030.
- Cao, Z., et al., 2023c. Ultra-High-Energy Gamma-Ray Astronomy. *Annual Review of Nuclear and Particle Science* 73, 341–363. URL: <https://doi.org/10.1146/annurev-nucl-112822-025357>, doi:10.1146/annurev-nucl-112822-025357, arXiv:https://doi.org/10.1146/annurev-nucl-112822-025357.
- Cardillo, M., Giuliani, A., 2023. The LHAASO PeVatron Bright Sky: What We Learned. *Appl. Sci.* 13, 6433. doi:10.3390/app13116433.
- Casanova, S., 2022. On the Search for the Galactic PeVatrons by Means of Gamma-Ray Astronomy. *Universe* 8, 505. doi:10.3390/universe8100505.
- Celli, S., Aharonian, F., Gabici, S., 2020. Spectral signatures of PeVatrons. *The Astrophysical Journal* 903, 61. URL: <https://doi.org/10.3847/1538-4357/abb805>, doi:10.3847/1538-4357/abb805.
- Celli, S., Morlino, G., Gabici, S., Aharonian, F.A., 2019. Exploring particle escape in supernova remnants through gamma rays. *MNRAS* 490, 4317–4333. URL: <https://doi.org/10.1093/mnras/stz2897>, doi:10.1093/mnras/stz2897, arXiv:https://academic.oup.com/mnras/article-pdf/490/3/4317/5077445/22971001.pdf.
- Chen, Y., et al., 2022. Chapter 2 galactic gamma-ray sources. *Chinese Physics C* 46, 030002. URL: <http://hepnp.ihep.ac.cn/en/article/doi/10.1088/1674-1137/ac3fa8>, doi:10.1088/1674-1137/ac3fa8.
- Cherenkov Telescope Array Consortium, Acharya, B.S., others, 2019. Science with the Cherenkov Telescope Array. *WORLD SCIENTIFIC*. doi:10.1142/10986.
- Clark, J. S., Negueruela, I., Crowther, P. A., Goodwin, S. P., 2005. On the massive stellar population of the super star cluster Westerlund 1. *A&A* 434, 949–969. URL: <https://doi.org/10.1051/0004-6361/20042413>, doi:10.1051/0004-6361/20042413.
- Coleman, A., 2019. Measurement of the Cosmic Ray Flux near the Second Knee with the Pierre Auger Observatory, in: 36th International Cosmic Ray Conference (ICRC2019). 24 July - 1 August 2019. Wisconsin, WI, p. PoS(ICRC2019)1177.
- Conceição, R., SWGO Collaboration, 2023. The Southern Wide-field Gamma-ray Observatory, in: 38th International Cosmic Ray Conference (ICRC2023). 26 July-3 August 2023. Nagoya, p. PoS(ICRC2023)963.
- Conceição, R., et al., 2021. Gamma/hadron discrimination using a small-WCD with four PMTs. *PoS ICRC2021*, 707. doi:10.22323/1.395.0707.
- Cristofari, P., 2021. The Hunt for Pevatrons: The Case of Supernova Remnants. *Universe* 7, 324. doi:10.3390/universe7090324, arXiv:2110.07956.
- Cristofari, P., Blasi, P., Amato, E., 2020. The low rate of Galactic pevatrons. *Astroparticle Physics* 123, 102492. doi:10.1016/j.astropartphys.2020.102492, arXiv:2007.04294.
- CTA Observatory and Consortium, 2021. CTAO Instrument Response Functions - prod5 version v0.1, <https://doi.org/10.5281/zenodo.5499840>. URL: <https://doi.org/10.5281/zenodo.5499840>, doi:10.5281/zenodo.5499840.
- Deil, C., et al., 2020. gammapy/gammapy: v.0.18.2 URL: <https://doi.org/10.5281/zenodo.4701500>, doi:10.5281/zenodo.4701500.
- Di Sciascio, G., 2022. Measurement of Energy Spectrum and Elemental Composition of PeV Cosmic Rays: Open Problems and Prospects. *Applied Sciences* 12. URL: <https://www.mdpi.com/2076-3417/12/2/705>, doi:10.3390/app12020705.
- Doro, M., SWGO Collaboration, 2022. The search for high altitude sites in South America for the SWGO detector, in: 37th International Cosmic Ray Conference (ICRC2021). 12-13 July 2021. Berlin, p. PoS(ICRC2021)689.
- Fang, K., 2022. Gamma-ray pulsar halos in the Galaxy. *Frontiers in Astronomy and Space Sciences* 9. URL: <https://www.frontiersin.org/articles/10.3389/fspas.2022.1022100>, doi:10.3389/fspas.2022.1022100.
- la Fuente, E.D., Flores, J.L., Garc'ia-Tor'ales, G., D'iaz-V'elez, J.C., Toledano-Ju'arez, I., Collaboration, T.H., 2023. The PeVatrons and the HAWC Observatory in Mexico. URL: <https://api.semanticscholar.org/CorpusID:259137394>.
- Gabici, S., Aharonian, F.A., 2007. Searching for Galactic Cosmic-Ray Pevatrons with Multi-TeV Gamma Rays and Neutrinos. *ApJL* 665, L131–L134. doi:10.1086/521047, arXiv:0705.3011.
- Giuliani, A., 2011. Neutral pion emission from accelerated protons in the supernova remnant W44. *ApJL* 742, 30. doi:10.1088/2041-8205/742/2/L30.
- Guépin, Claire, Cerutti, Benoît, Kotera, Kumiko, 2020. Proton acceleration in pulsar magnetospheres. *A&A* 635, A138. doi:10.1051/0004-6361/201936816.
- H. E. S. S. Collaboration, Abdalla, H., others, 2018. The H.E.S.S. Galactic plane survey. *A&A* 612, A1. doi:10.1051/0004-6361/201732098, arXiv:1804.02432.
- HESS Collaboration, Abramowski, A., others, 2016. Acceleration of petaelectronvolt protons in the Galactic Centre. *Nature* 531, 476–479. doi:10.1038/nature17147, arXiv:1603.07730.
- Higdon, J.C., Lingenfelter, R.E., 2003. The Superbubble Origin of 22-Ne in Cosmic Rays. *ApJ* 590, 822–832. doi:10.1086/375192.
- Hinton, J., SWGO Collaboration, 2022. The Southern Wide-field Gamma-ray Observatory: Status and Prospects, in: 37th International Cosmic Ray Conference (ICRC2021). 12-23 July 2021. Berlin, p. PoS(ICRC2021)023. arXiv:2111.13158.
- Hofmann, W., 2020. On angular resolution limits for air shower arrays. *Astroparticle Physics* 123, 102479. URL: <https://www.sciencedirect.com/science/article/pii/S0927650520300517>, doi:https://doi.org/10.1016/j.astropartphys.2020.102479.
- Hofmann, W., et al., 2023. The Cherenkov Telescope Array doi:10.48550/arXiv.2305.12888, arXiv:2305.12888v1.
- Kafexhiu, E., Aharonian, F., Taylor, A.M., Vila, G.S., 2014. Parametrization of gamma-ray production cross sections for p-p interactions in a broad proton energy range from the kinematic threshold to PeV energies. *Phys. Rev. D* 90, 123014. doi:10.1103/PhysRevD.90.123014, arXiv:1406.7369.
- Kelner, S.R., Aharonian, F.A., Bugayov, V.V., 2006. Energy spectra of gamma rays, electrons, and neutrinos produced at proton-proton interactions in the very high energy regime. *Phys. Rev. D* 74, 034018. URL: <https://link.aps.org/doi/10.1103/PhysRevD.74.034018>, doi:10.1103/PhysRevD.74.034018.
- Kunwar, S., 2021. Double-layered Water Cherenkov Detector for SWGO. *PoS ICRC2021*, 902. doi:10.22323/1.395.0902.
- La Mura, G., Chiaro, G., Conceição, R., De Angelis, A., Pimenta, M., Tome, B., 2020. Detection of very-high-energy gamma-ray transients with monitoring facilities. *MNRAS* 497, 3142–3148. doi:doi.org/10.1093/mnras/staa2141.
- Lang, R.G., SWGO Collaboration, 2023. Estimating the potential of SWGO to measure the composition-dependent behaviour of the CR anisotropy, in: 38th International Cosmic Ray Conference (ICRC2023). 26 July-3 August 2023. Nagoya, p. PoS(ICRC2023)486.
- LHAASO Collaboration, Cao, Z., et al., 2021. Peta-electron volt gamma-ray emission from the Crab Nebula. *Science* 373, 425–430. doi:10.1126/science.abg5137, arXiv:2111.06545.
- Linden, T., Auchettl, K., Bramante, J., Cholis, I., Fang, K., Hooper, D., Karwal, T., Li, S.W., 2017. Using HAWC to discover invisible pulsars. *Phys. Rev. D* 96, 103016. URL: <https://link.aps.org/doi/10.1103/PhysRevD.96.103016>, doi:10.1103/PhysRevD.96.103016.
- Magee, P., et al., 2021. First Demonstration of Early Warning Gravitational-wave Alerts. *ApJL* 910, L21. doi:10.3847/2041-8213/abed54, arXiv:2102.04555.
- MAGIC Collaboration, Abe, H., et al., 2023. MAGIC observations provide compelling evidence of hadronic multi-TeV emission from the putative PeVatron SNR G106.3+2.7. *A&A* 671, A12. URL: <https://doi.org/10.1051/0004-6361/202244931>, doi:10.1051/0004-6361/202244931.
- Marcowith, A., et al., 2018. Core-collapse supernovae as cosmic ray sources. *MNRAS* 479, 4470–4485. doi:10.1093/mnras/sty1743, arXiv:1806.09700.
- Meneguolo, C., Bernardini, E., Mancina, S., 2023. Sentinel of the extraordinary: the IceCube alert system for neutrino flares, in: 38th International Cosmic Ray Conference (ICRC2023). 26 July - 3 August 2023. Nagoya, Japan., p. PoS(ICRC2023)1500. arXiv:2307.15501.
- Morlino, G., Blasi, P., Peretti, E., Cristofari, P., 2021. Particle acceleration in winds of star clusters. *MNRAS* 504, 6096–6105. URL: <https://doi.org/10.1093/mnras/stab690>, doi:10.1093/mnras/stab690, arXiv:https://academic.oup.com/mnras/article-pdf/504/4/6096/3824152.
- Ohira, Y., Kisaka, S., Yamazaki, R., 2018. Pulsar Wind Nebulae inside Supernova Remnants as Cosmic-Ray PeVatrons. *MNRAS* 478, 926–931. doi:doi.org/10.1093/mnras/sty1159, arXiv:1702.05866.
- Santander, M., SWGO Collaboration, 2023. An update on site search activities

for SWGO, in: 38th International Cosmic Ray Conference (ICRC2023). 26 July-3 August 2023. Nagoya, p. PoS(ICRC2023)752.

Schoorlemmer, H., SWGO Collaboration, 2022. Simulating the performance of the Southern Wide-view Gamma-ray Observatory, in: 37th International Cosmic Ray Conference (ICRC2021). 12-13 July 2021. Berlin, p. PoS(ICRC2021)903.

Schroder, F., 2019. News from Cosmic Ray Air Showers (ICRC 2019 – Cosmic Ray Indirect Rapport), in: 36th International Cosmic Ray Conference (ICRC2019). 24 July - 1 August 2019. Wisconsin, WI, p. PoS(ICRC2019)030.

Schure, K.M., Bell, A.R., 2013. Cosmic ray acceleration in young supernova remnants. *MNRAS* 435, 1174–1185. doi:10.1093/mnras/stt1371, arXiv:1307.6575.

Spengler, G., 2020. Search for Galactic Pevatron candidates in a population of unidentified sources. *A&A* 633, A138. URL: <https://doi.org/10.1051/0004-6361/201936632>, doi:10.1051/0004-6361/201936632.

Spengler, G., 2022. ecpli python package. <https://github.com/dvn11/ecpli>. Accessed: 2022-08-04.

Sudoh, T., Beacom, J.F., 2023. Where are Milky Way’s hadronic PeVatrons? *Phys. Rev. D* 107, 043002. URL: <https://link.aps.org/doi/10.1103/PhysRevD.107.043002>, doi:10.1103/PhysRevD.107.043002.

Tatischeff, V., 2009. Radio emission and nonlinear diffusive shock acceleration of cosmic rays in the supernova SN 1993J. *A&A* 499, 191–213. doi:10.1051/0004-6361/200811511.

Vernetto, S., for the LHAASO Collaboration, 2016. Gamma Ray Astronomy with LHAASO. *Journal of Physics: Conference Series* 718, 052043. URL: <https://dx.doi.org/10.1088/1742-6596/718/5/052043>, doi:10.1088/1742-6596/718/5/052043.

Vernetto, S., Lipari, P., 2016. Absorption of very high energy gamma rays in the Milky Way. *Phys. Rev. D* 94, 063009. doi:10.1103/PhysRevD.94.063009, arXiv:1608.01587.

Vieu, T., Reville, B., Aharonian, F., 2022. Can superbubbles accelerate ultra-high energy protons? *MNRAS* 515, 2256–2265. doi:doi.org/10.1093/mnras/stac1901, arXiv:2207.01432.

Vink, J., 2022. What sources are the dominant Galactic cosmic-ray accelerators? arXiv e-prints, arXiv:2212.10677doi:10.48550/arXiv.2212.10677, arXiv:2212.10677.

della Volpe, D., 2023. Highlights from the large high-altitude air-shower observatory (lhaaso). *Journal of Physics: Conference Series* 2429, 012014. URL: <https://dx.doi.org/10.1088/1742-6596/2429/1/012014>, doi:10.1088/1742-6596/2429/1/012014.

Yang, R., Kafexhiu, E., Aharonian, F., 2018. Exploring the shape of the gamma-ray spectrum around the pi0-bump. *A&A* 615, A108. URL: <https://doi.org/10.1051/0004-6361/201730908>, doi:10.1051/0004-6361/201730908.

Zabarov, D., the Baikal-GDV Collaboration, 2021. High-energy neutrino astronomy and the Baikal-GVD neutrino telescope. *Phys. Atom. Nuclei* 84, 513. doi:10.48550/arXiv.2011.09209, arXiv:2011.09209.

Zirakashvili, V.N., Ptuskin, V.S., 2016. Type II_n supernovae as sources of high energy astrophysical neutrinos. *Astroparticle Physics* 78, 28–34. doi:10.1016/j.astropartphys.2016.02.004.